Quaternary Science Reviews 134 (2016) 59–73

Contents lists available at ScienceDirect

Quaternary Science Reviews

journal homepage: www.elsevier.com/locate/quascirev

Luminescence dating of glacial advances at Lago Buenos Aires (~46 °S), Patagonia

R.K. Smedley*, N.F. Glasser, G.A.T. Duller

Department of Geography and Earth Sciences, Aberystwyth University, Ceredigion, SY23 3DB, UK

ARTICLE INFO

Article history:
Received 21 July 2015
Received in revised form
3 December 2015
Accepted 15 December 2015
Available online 13 January 2016

Keywords:
Patagonia
Glacial
Geomorphology
Luminescence
Single grains
Feldspar

ABSTRACT

Understanding the timing of past glacial advances in Patagonia is of global climatic importance because of the insight this can provide into the influence on glacier behaviour of changes in temperature and precipitation related to the Southern Westerlies. In this paper we present new luminescence ages determined using single grains of K-feldspar from proglacial outwash sediments that were deposited by the Patagonian Ice Sheet around Lago Buenos Aires (~46 °S), east of the contemporary Northern Patagonian Icefield. The new luminescence ages indicate that major outwash accumulations formed around ~110 ± 20 ka to 140 ± 20 ka and that these correspond to the Moreno I and II moraine ridges, which were previously dated using cosmogenic isotope dating to 150 ± 30 ka. Luminescence dating at Lago Buenos Aires has also identified outwash sediments that were deposited during glacial advances ~30.8 ± 5.7 ka and ~34.0 ± 6.1 ka (MIS 3) that are not recorded in the moraine record. Younger outwash accumulations were then deposited between ~14.7 ± 2.1 and 26.2 ± 1.6 ka which correspond to the Fenix I – V moraine ridges. The combined chronology suggests that glacial advances occurred ~110 ± 20 ka to 150 ± 30 ka (MIS 6), ~30.8 ± 5.7 ka to ~34.0 ± 6.1 ka (MIS 3), and ~14.7 ± 2.1 to 26.2 ± 1.6 ka (MIS 2) at Lago Buenos Aires. Overall luminescence dating using single grains of K-feldspar has excellent potential to contribute towards the ever-increasing geochronological dataset constraining the timings of glacial advances in Patagonia.

1. Introduction

Providing robust age constraints for the timing of past glacial advances can offer an important contribution to the global climate change debate. Empirical datasets constraining climate change of the past can be used to test numerical models. Terrestrial climates in the mid-latitudes of the Southern Hemisphere are of global climatic importance because of the influence of the precipitation-bearing Southern Westerlies between latitudes of ~30 and 55 °S, with the position of the present-day core of the Southern Westerlies at ~50 to 55 °S (Lamy et al., 2010). A large Patagonian Ice Sheet is known to have extended along the Andean mountain range from ~38 °S to 56 °S during repeated glacial cycles of the Quaternary period (e.g. Glasser et al., 2008). This ice sheet may have fluctuated in response to potential changes in precipitation supply related to the migration of the Southern Westerlies (e.g. Denton et al., 1999; Hulton et al., 1994). Providing accurate and precise age constraints on past glacial advances of the Patagonian Ice Sheet can be used to test the accuracy of ice-sheet models, and consequently improve our understanding of how the Earth responds to long-term climatic change. However, providing age constraints for glacial advances of the past can be challenging as some geochronological techniques are restricted by material availability and age ranges, but can also be restricted by processes that have occurred since deposition. The most effective approach to produce robust chronologies in glaciated settings is to combine datasets which use multiple dating techniques to provide ages (e.g. radiocarbon, cosmogenic isotope and luminescence dating). Moreover, researchers are now beginning to incorporate these age sequences into Bayesian frameworks to model patterns of glacial advance and retreat (e.g. Chiverrell et al., 2013).

Luminescence dating is a technique that can determine the last time a grain of sand was exposed to sunlight prior to burial and has great potential for directly dating the sediment deposited during a glacial advance. The luminescence dating technique depends on the ability of mineral grains (typically either quartz or K-feldspars) to store energy within the crystalline structure of the grain and

* Corresponding author.
E-mail address: rks09@aber.ac.uk (R.K. Smedley).

http://dx.doi.org/10.1016/j.quascirev.2015.12.010

release it upon stimulation (e.g. exposure to sunlight). Upon exposure to sunlight the signal used for luminescence dating is reset (or bleached) before the grains are then buried, where they are exposed to natural radiation from the surrounding environment (e.g. Rhodes, 2011). Luminescence dating is most suitable for providing ages in well-bleached settings (e.g. aeolian) where the opportunity for sunlight exposure is greater than in glaciofluvial or fluvial settings. In comparison to aeolian settings, the luminescence signal of mineral grains from glaciofluvial settings is typically partially bleached as there is greater potential for shorter sediment transport pathways and attenuation of light through the turbulent, sediment-laden water columns transporting the grains (Berger and Luternauer, 1987). Glaciofluvial sediments are typically targeted in glaciated settings to maximise the opportunity for exposure to sunlight, which is greater than expected for sediments deposited as a moraine (e.g. Fuchs and Owen, 2008; Thrasher et al., 2009a). Luminescence dating of single grains can then be used to assess whether heterogeneous bleaching of the luminescence signal from individual grains has occurred and determine accurate ages by applying relevant statistical age models (Duller, 2008; Galbraith and Roberts, 2012).

A major challenge for single-grain dating of quartz from glaciated environments is that commonly only 5% or fewer of the grains emit a detectable optically stimulated luminescence (OSL) signal, and in glaciofluvial sediments from Chile as few as 0.5% of quartz grains could be detected (Duller, 2006). In contrast, a larger proportion of K-feldspar grains emit a detectable infra-red stimulated luminescence (IRSL) signal, which is typically brighter than the OSL signal emitted from quartz grains (e.g. Duller et al., 2003). Single-grain dating using K-feldspar therefore has the potential to make luminescence dating more efficient and potentially more precise in environments that are characterised by short sediment transport pathways, and also in regions where the sensitivity of the quartz is poor e.g. glaciofluvial sediments (Duller, 2006).

Currently, OSL dating of quartz is more commonly applied for routine dating of single grains as the IRSL signal of K-feldspars is prone to the effects of anomalous fading (Wintle, 1973). Anomalous fading is the athermal depletion of the luminescence signal over time and if fading is not accurately measured and corrected for, it will manifest as an underestimation of the burial age. There are two signals commonly used for IRSL dating of K-feldspars; (1) the IRSL signal typically measured at 50 °C, termed the IR_{50} signal (e.g. Wallinga et al., 2000), and (2) the post-IR IRSL signal typically measured at 225 °C or 290 °C, termed the $pIRIR_{225}$ and $pIRIR_{290}$ signals (Thomsen et al., 2008, 2011). Anomalous fading of the IR_{50} signal is suggested by some workers to be ubiquitous to all feldspars (e.g. Huntley and Lamothe, 2001), whereas the pIRIR signal is suggested to access a more stable signal through the recombination of more distal donor-acceptor electron pairs (Jain and Ankjærgaard, 2011). Accessing a more stable IRSL signal within the K-feldspar grains for dating is advantageous as it reduces the influence of anomalous fading on the age calculation, which is especially important on a single grain level, where accurate and precise measurement and correction for fading can be difficult. Few studies have determined ages for sedimentary samples from the natural environment using the pIRIR signal of single grains of K-feldspar (e.g. Gaar et al., 2014; Trauerstein et al., 2014). However, studies have demonstrated that the pIRIR signal can provide ages in direct agreement with independent numerical age control for well-bleached samples (e.g. Reimann et al., 2012; Smedley, 2014).

The aim of this paper is to test the new luminescence dating technique using single grains of K-feldspar from proglacial sediments and complement the pre-existing chronology provided by cosmogenic isotope (Kaplan et al., 2005, 2011) and $^{40}Ar/^{39}Ar$ (Singer et al., 2004) dating at Lago Buenos Aires. The combined chronology will strengthen the age constraints provided for the glacial advances as it can provide checks on the internal consistency between techniques and also provide ages for different landforms preserved after deglaciation.

2. Study site and sample descriptions

In the past a large outlet glacier expanded eastwards at Lago Buenos Aires from the Andean mountain range on to the semi-arid Argentine plateau (Caldenius, 1932). Multiple sets of moraine ridges are preserved in the valley, extending from the Last Glacial Maximum (LGM) to ~1 million years ago (Ma). The moraine complexes are locally named the Menucos (I), Fenix (I – V), Moreno (I – III), Deseado (I – III) and Telken (I – VII) moraines, ordered from youngest to oldest. Age constraints for the glacial advances are currently provided by cosmogenic isotope dating of moraine boulders (Kaplan et al., 2004, 2005, 2011; Douglass et al., 2006) and $^{40}Ar/^{39}Ar$ dating of the basaltic lava flows (Singer et al., 2004). The timing of the LGM at Lago Buenos Aires is recorded by the deposition of the Fenix moraine ridges and is suggested to have been broadly synchronous with sites across Patagonia from ~16 to 30 ka (Kaplan et al., 2004, 2011; Douglass et al., 2006), and with the responses of global ice sheets (e.g. Mix et al., 2001; Glasser et al., 2011). The Moreno and Deseado moraines are suggested to predate the LGM at Lago Buenos Aires (Kaplan et al., 2005).

Well preserved proglacial outwash plains (or sandur) at Lago Buenos Aires were targeted for luminescence dating. The low-angled slope of each outwash plain can be traced eastwards from the former ice front marked by the prominent moraine ridge. These proximal outwash plains can only have been active when the ice front was positioned at the elevation marked by the corresponding moraine ridge. Assessing the geomorphological and sedimentological context of each luminescence sample enables a direct comparison to be made between the luminescence and cosmogenic isotope ages. The geomorphology at Lago Buenos Aires was mapped in this study using Landsat imagery in combination with Google Earth imagery and ground truthing in Patagonia (Fig. 1). Differential Global Positioning System (dGPS) measurements of altitude, latitude and longitude were also used to develop an elevation profile at Lago Buenos Aires and a conceptual model describing the possible development of the sedimentary sequence for the Menucos and Fenix moraines (Fig. 2). The relationship between the moraine ridges and outwash plains that were sampled is shown by the elevation profiling and conceptual model (Fig. 2). The re-activation of pre-existing glaciofluvial channels and the presence of glaciofluvial channels that were orientated NW-SE, draining laterally across the valley and in front of the moraine ridges (Fig. 1) complicated these relationships for some samples; this will be discussed later in Section 2.1. Cosmogenic isotope dating of the moraine ridges suggest that each moraine and related outwash plain was deposited during different glacial advances or still-stands (Kaplan et al., 2004, 2011).

Luminescence dating was performed on 13 sedimentary samples taken at Lago Buenos Aires. The locations of the luminescence samples associated with the Fenix (n = 9 samples), Moreno (n = 3 samples) and Deseado (n = 1 sample) moraine complexes are shown with the location of the existing chronology (Fig. 1). The elevation profile (Fig. 2) shows the difference in elevation (~50 m) of the Fenix and Moreno moraine complexes, and the Moreno and Deseado moraine complexes (also ~50 m). Table 1 presents the details of the samples taken for luminescence dating and each sample site is shown in Fig. 3, where the moraine fragments and outwash plains related to each of the luminescence samples are highlighted in relation to Fig. 2.

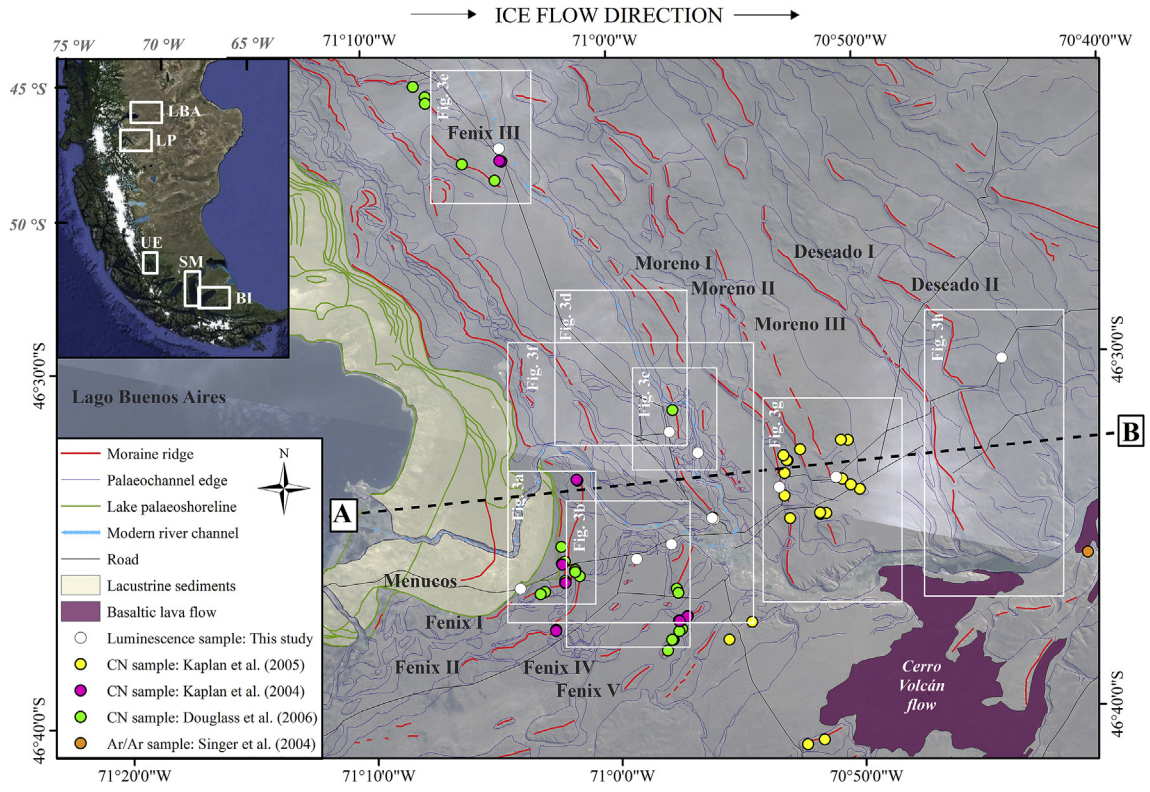

Fig. 1. Location of Lago Buenos Aires, Patagonia (GoogleEarth; Image © Landsat) and geomorphological map which includes the sites sampled for luminescence dating, the existing chronology and the locations of the images in Fig. 3. The inset shows the locations in South America of Lago Buenos Aires (LBA), Lago Pueyrrédon (LP), the Última Esperanza region (UE), the Strait of Magellan (SM) and Bahia Inútil (BI).

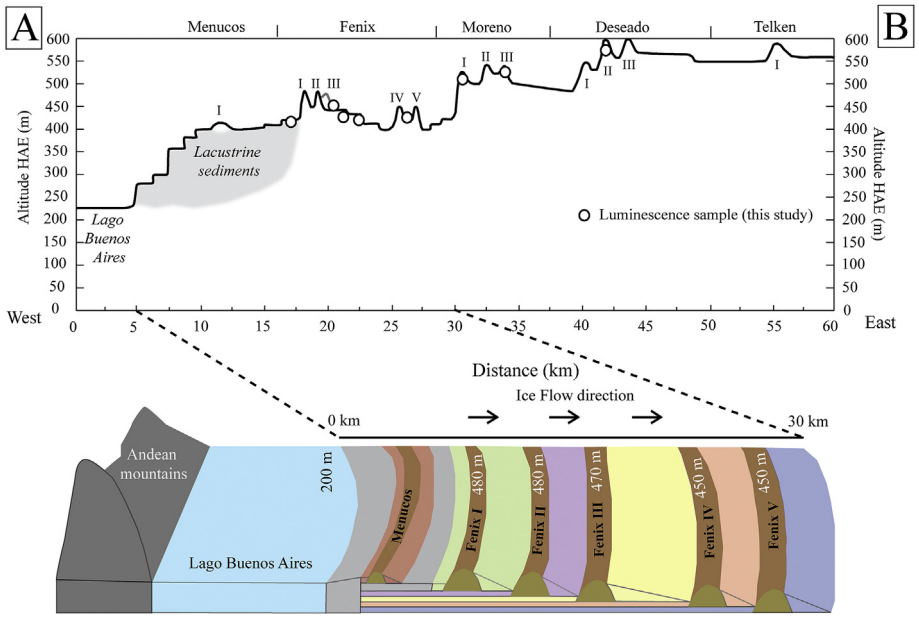

Fig. 2. Elevation profile created from altitudes (HAE – Height Above Ellipsoid), latitudes and longitudes determined using dGPS measurements along line A to B in Fig. 1. Also shown is a schematic diagram of the Menucos and Fenix moraine ridges with associated outwash plains at Lago Buenos Aires.

2.1. Fenix moraines

The geomorphological and sedimentological contexts of four of the nine samples related to the Fenix moraines were typical of a proglacial outwash plain deposited in front of a moraine ridge (samples LBA12OW3 – Fig. 3a; LBA12OW4 – Fig. 3b; LBA12OW1 – Fig. 3d; and LBA12OW2 – Fig. 3e). The sediments were either poorly sorted (samples LBA12OW4 or LBA12OW2), which is typical of higher energy glaciofluvial depositional conditions, or well sorted (LBA12OW3 and LBA12OW1), which is typical of stagnant water

Table 1
Samples taken for luminescence dating from outwash sediments at Lago Buenos Aires, Patagonia.

Sample	Location	Elevation (m)	Moraine association	All grains		20% brightest grains		Age model	D_e value (Gy)	Age (ka)
				n	Overdisp. (%)	n	Overdisp. (%)			
LBA12OW3	46°36.37 W 71°04.00 S	410	>Menucos & ≤Fenix I	156	43.1 ± 0.2	31	38.6 ± 0.9	CAM	66.1 ± 4.6	14.7 ± 2.1
LBA12OW5	46°35.23 W 70°57.78 S	415	≤Fenix II	162	80.2 ± 0.4	28	79.0 ± 1.8	MAM	73.0 ± 14.0	20.2 ± 4.5
LBA12RF1	46°32.66 W 70°56.61 S	414	≤Fenix II	250	55.9 ± 0.2	41	57.7 ± 0.8	MAM	123.3 ± 16.8	34.0 ± 6.1
LBA12OW1	46°32.05 W 70°57.75 S	426	Fenix II	179	38.9 ± 0.2	36	26.1 ± 0.6	CAM	61.2 ± 2.8	18.5 ± 2.4
LBA12OW4	46°35.62 W 70°59.21 S	439	Fenix II	154	89.1 ± 0.4	29	71.0 ± 1.7	MAM	68.3 ± 15.4	20.5 ± 5.3
LBA12OW2	46°23.92 W 70°04.73 S	502	Fenix III	226	70.7 ± 0.2	43	66.2 ± 1.0	MAM	78.3 ± 13.9	22.3 ± 4.8
LBA12F4-2	46°34.51 W 70°56.08 S	386	≥Fenix IV	260	71.6 ± 0.1	45	68.2 ± 1.0	MAM	115.4 ± 16.1	30.8 ± 5.7
LBA12F4-3	46°34.51 W 70°56.08 S	386	>Fenix IV	250	45.8 ± 0.1	37	37.6 ± 0.6	CAM	489.2 ± 27.3	141 ± 19
LBA12F4-1	46°34.55 W 70°56.01 S	394	≤Fenix IV	244	67.2 ± 0.2	45	79.6 ± 1.2	MAM	67.4 ± 8.4	19.5 ± 3.3
LBA12M1-1	46°33.69 W 70°53.31 S	467	Moreno I	102	46.5 ± 0.3	46	39.4 ± 1.2	CAM	416.8 ± 34.1	132 ± 19
LBA12M1-2	46°33.69 W 70°53.31 S	467	Moreno I	136	59.8 ± 0.4	27	51.4 ± 1.7	CAM	493.7 ± 55.4	134 ± 22
LBA12M3	46°33.44 W 70°50.97 S	510	Moreno III	109	50.4 ± 0.1	22	40.9 ± 1.5	CAM	365.0 ± 34.0	111 ± 17
LBA12D2-1	46°30.18 W 70°44.10 S	556	Deseado II	122	40.1 ± 0.3	25	42.3 ± 1.4	CAM	437.4 ± 39.6	123 ± 18

CAM = Central Age Model; MAM = Minimum Age Model (3-parameter).

conditions. The outwash sediments of all four of these samples were part of proximal outwash plains with low-angled slopes that can be traced westwards to the moraine ridge where the ice front was positioned when the outwash plain was active. The outwash plain of sample LBA12OW3 (410 m elevation) was eroded by the lake shorelines and lacustrine sediments that underlie the Menucos moraine ridge (Fig. 3a). The outwash plain was also constrained to the east by the Fenix I moraine ridge which has been eroded by a glaciofluvial channel at an elevation of 410 m. The age of the outwash plain of sample LBA12OW3 must therefore be older than the Menucos moraine and younger than the Fenix I moraine (Table 1).

The outwash plain of sample LBA12OW4 (440 m) was elevated 30 m higher than the outwash plain of sample LBA12OW3 (410 m), and was likely active during an earlier phase of glaciation. The sediments dated for sample LBA12OW4 were collected from ~2 km in front of the Fenix II moraine, where the ice front was positioned at an elevation of ~470 m when the sediment was deposited (Fig. 3b). The outwash plain of sample LBA12OW4 was therefore active when the ice front was positioned ~2 km to the west at the Fenix II moraine (Table 1). Sample LBA12OW1 was taken from a small section of an outwash plain ~3 km in length and ~0.2 km wide that was constrained to the east by the Fenix IV moraine ridge and truncated to the west by a younger, lower (by ~10 m) glaciofluvial channel draining from the north (Fig. 3d). The low-angled slope of the outwash plain can be traced at an elevation of 450 m for ~8 km from the Fenix II moraine ridge to the location of sample LBA12OW1. Similar to the outwash plain of sample LBA12OW4 elevated at 440 m, the outwash plain of sample LBA12OW1 was also likely to have been active when the ice front was positioned at the Fenix II moraine ridge (470 m elevation).

To the east of the Fenix II moraine are the poorly preserved fragments of the Fenix III moraine and proximal outwash plains (Fig. 3e). The landform targeted for sample LBA12OW2 was an outwash plain that extended for <1 km eastwards from the Fenix III moraine as a low-angled slope at an elevation of 500 m (Fig. 3e). Sample LBA12OW2 was taken from ~0.5 m in front of the moraine ridge within this outwash plain. The close proximity and elevation of the outwash plain of sample LBA12OW2 suggests that this was active when the ice front was positioned at the Fenix III moraine (Table 1).

The geomorphological contexts of the other sample sites related to the Fenix moraines were more complex. The sedimentary units that samples LBA12OW5, LBA12RF1, LBA12F4-1 and LBA12F4-2 were taken from were all poorly sorted, but it was difficult to directly link these samples to specific moraine ridges using the geomorphology. Based on the elevation profile of the outwash plains, samples LBA12OW5 and LBA12RF1 are interpreted to have been deposited at a similar time or before the Fenix II moraine ridge. However, the conceptual model (Fig. 2) suggests that it is possible for sediments from younger glacial advances to have been deposited on top of sediments from older glacial advances. Glaciofluvial sediments preserved at different elevations at a single site may therefore have recorded multiple glacial advances within the same stratigraphy, whereas the more prominent moraine ridges relating to older glaciations were likely destroyed by overriding ice. Therefore, it is possible that the proglacial sediments sampled for luminescence dating at lower elevations within the sedimentary sequence may be older than the moraine ridges themselves.

Samples LBA12F4-2 and LBA12F4-3 were extracted from the same stratigraphic section (Fig. 4a), ~100 m west of sample LBA12F4-1 (Fig. 4b). The context of these three samples is complicated due to their proximity to the central glaciofluvial channel in the valley, which was re-activated during younger glaciations. Also, post- or syn-depositional processes have deformed some of the sediments in these sections and complicated the stratigraphy (Fig. 4a). The stratigraphy of the site is outwash gravel units deformed by a silty-sand unit that contained rounded pebbles, which is interpreted to be lacustrine sediments deposited in a proglacial lake setting. After deposition, the preserved lake

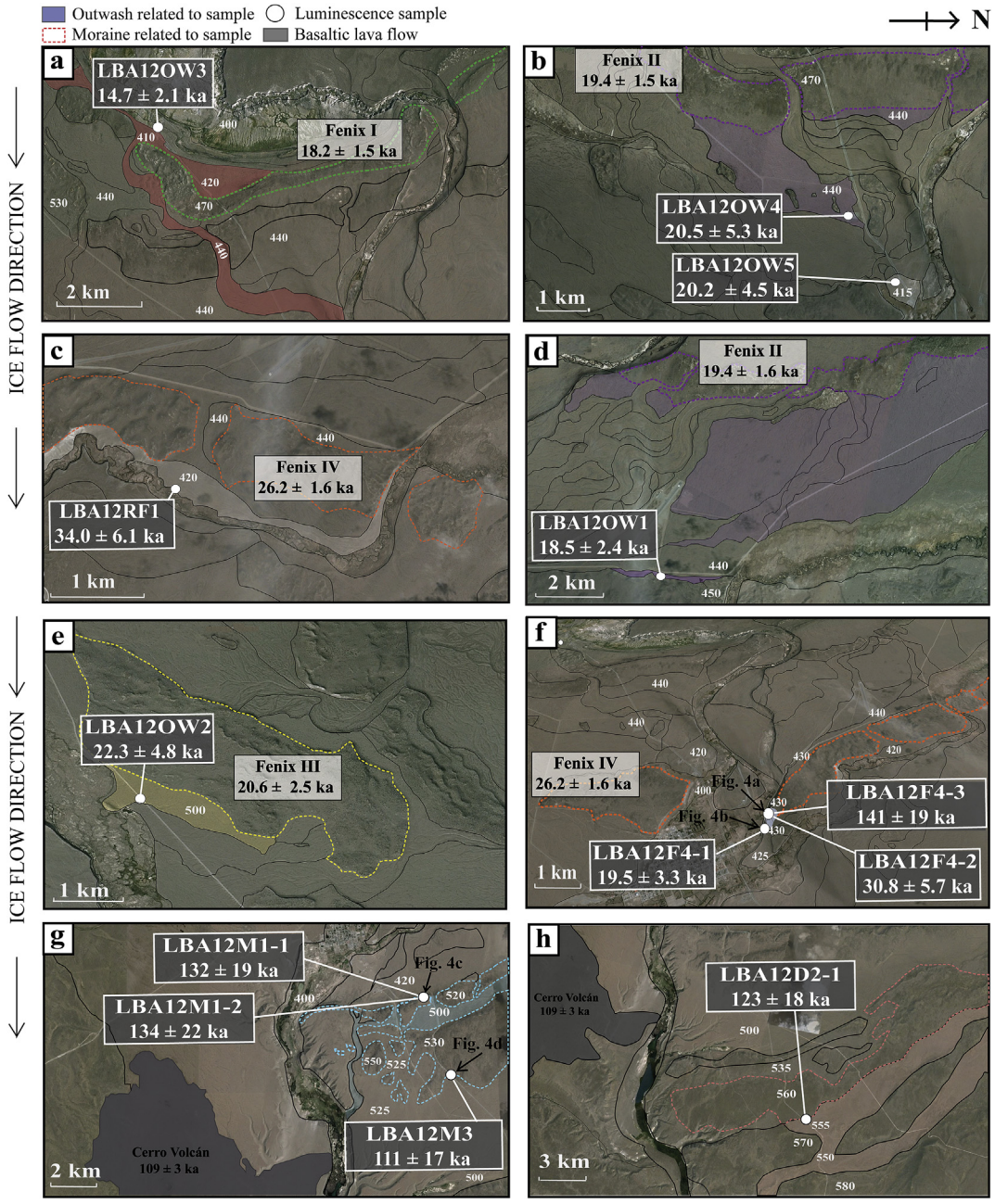

Fig. 3. Annotated GoogleEarth images (Image © 2014 CNES/Astrium) showing the geomorphological relationship between the moraine ridges and outwash sediments used for luminescence dating from Lago Buenos Aires; the colours of the landforms relate to Fig. 2. White shading indicates where the relationship between the outwash plain and moraine ridge for a sample was difficult to determine. The locations of the different images are shown on Fig. 1. The elevation measurements determined for the different outwash plain levels using the dGPS are shown in white. The cosmogenic isotope ages determined for each moraine ridge (Kaplan et al., 2011) and luminescence ages (this study) for associated outwash from this study are included in this figure. (For interpretation of the references to colour in this figure legend, the reader is referred to the web version of this article.)

sediments were thrust up into the overlying glaciofluvial sediment to an angle of ~40° (Fig. 4a). The sedimentary units were then covered by a laterally-extensive sedimentary sequence of horizontally-layered glaciofluvial sediments (up to ~2 m thick), diamicton (up to ~2 m thick), and ~0.5 m thick unit of glaciofluvial sediments.

The glaciofluvial sediments sampled for LBA12F4-1 were not deformed by post- or syn-depositional processes and were sampled at an elevation of ~434–438 m (Fig. 4b), which was similar to the upper sedimentary units (~436–440 m elevation) of the section sampled for LBA12F4-2 (Fig. 4a). The stratigraphy at these two sites suggests that multiple glacial advances have been preserved, which is consistent with the hypothetical conceptual model for the deposition of the Fenix moraines (Fig. 2). The glaciofluvial sediments deposited in the lower part of the section that have been deformed post- or syn-depositionally (sampled by LBA12F4-2) potentially relate to an older glacial advance, and the glaciofluvial sediments in the upper part of the sequence (sampled by LBA12F4-1) relate to a younger glacial advance, which is potentially related to the Fenix IV moraine ridge in this area (Fig. 3f). The glaciolacustrine sediments that sample LBA12F4-3 was taken from are stratigraphically older than both samples LBA12F4-1 and LBA12F4-2.

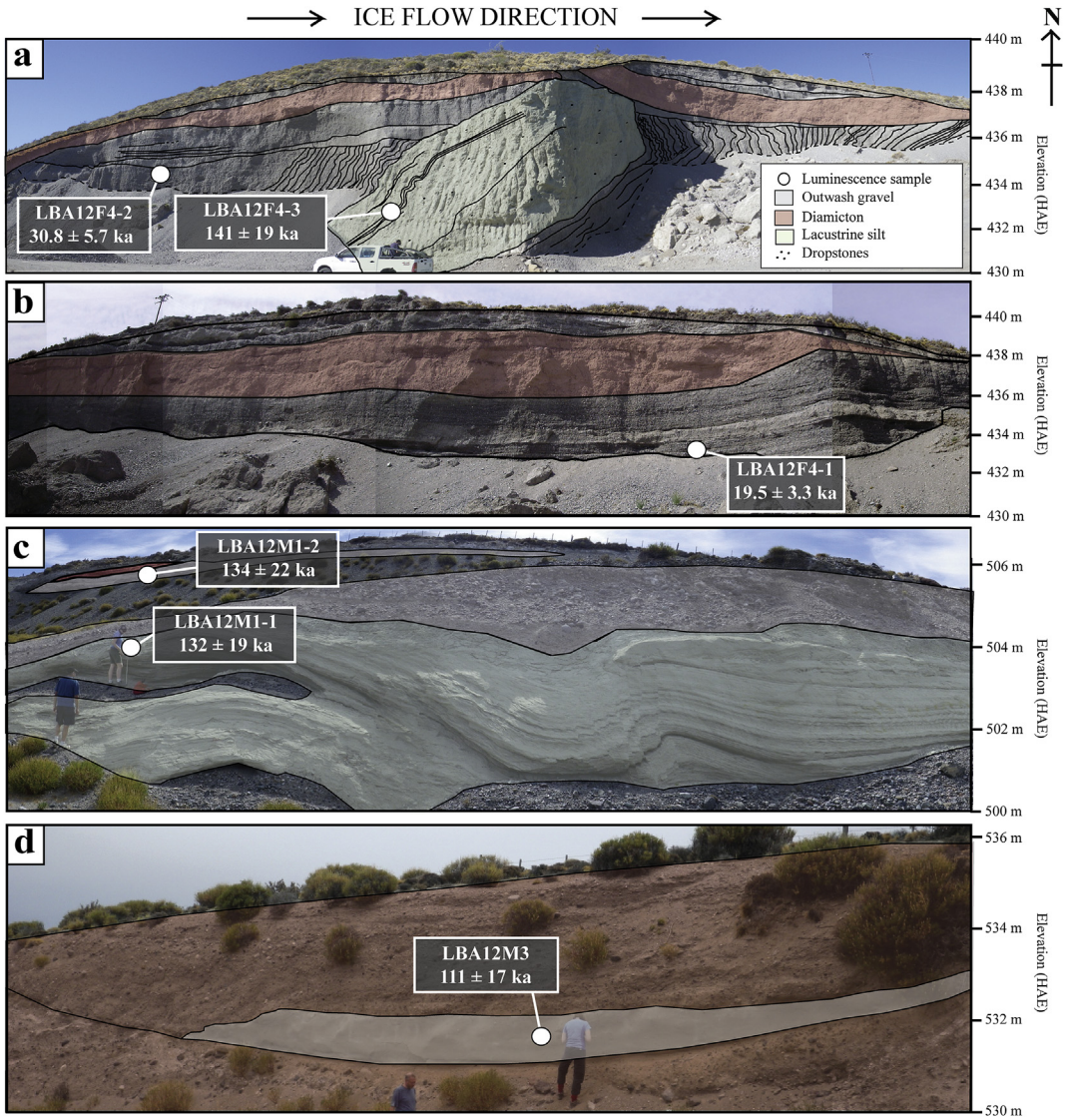

Fig. 4. Stratigraphical sections showing the outwash sediments sampled for LBA12F4-2 and LBA12F4-3 (a), LBA12F4-1 (b), LBA12M1-1 and LBA12M1-2 (c) and LBA12M3 (d). The stratigraphy shown in (a) includes a unit of lacustrine sediments (sampled by LBA12F4-3) thrust up into overlying outwash sediments (sampled by LBA12F4-2), which have been post- or syn-depositionally deformed. The section shown in (b) was ~100 m east of the section shown in (a), but the outwash sediments not deformed by post- or syn-depositional processes. Elevation measurements (HAE – Height Above Ellipsoid) for each section are from the dGPS measurements.

2.2. Moreno moraines

The three samples taken from glaciofluvial and glaciolacustrine sediments related to the Moreno moraines were from elevations >500 m (Fig. 3g; LBA12M1-1, LBA12M1-2 and LBA12M3). Samples LBA12M1-1 and LBA12M1-2 were taken from the same stratigraphic section, which was associated with the Moreno I moraine (Fig. 4c). Sample LBA12M1-1 was taken from glaciolacustrine sediments that were post-depositionally deformed and then covered by the glaciofluvial sediments that sample LBA12M1-2 was taken from, and so sample LBA12M1-1 therefore must have been deposited before sample LBA12M1-2. Sample LBA12M3 was taken from a well-sorted, coarse-grained sand unit deposited within a matrix-supported diamicton of the Moreno III moraine ridge (Fig. 4d). The sediments are interpreted to have been deposited in a ponded, slack water feature that formed as part of the Moreno III moraine ridge (Fig. 3g). The elevation profile (Fig. 2) suggests that the Moreno III moraine ridge and associated outwash plains sampled by LBA12M3 (530 m) were covered by the Cerro Volcán lava flow and should therefore be older than the $^{40}Ar/^{39}Ar$ age of 109 ± 3 ka.

3. Re-calculation of existing cosmogenic isotope ages

Cosmogenic isotope ages for the Moreno moraines calculated using earlier estimates of production rates suggest that these glacial advances occurred during Marine Isotope Stage (MIS) 6 (Kaplan et al., 2005). The ^{10}Be ages published in Kaplan et al. (2005) have been re-calculated in this study using the recently obtained production rates for mid-latitudes of the Southern Hemisphere, updates to scaling factors for location and altitude and other systemic improvements in the technique (see Balco et al., 2008; Kaplan et al., 2011). The production rate determined from south of Lago Argentino (Kaplan et al., 2011) is statistically identical to the production rate determined from the Southern Alps in New Zealand (Putnam et al., 2010). The re-calculated cosmogenic isotope ages suggest that the Moreno I and II moraine ridges are from MIS 6; the distribution of ages ranges from 108 ± 6 ka to 209 ± 11 ka, with

weighted mean and standard deviations of 148 ± 33 ka and 154 ± 35 ka, respectively (see Table S.1 for details).

4. Measurement of dose-rates for luminescence dating

Dose-rates are determined in luminescence dating to quantify the amount of natural radiation the mineral grains were exposed to per year throughout burial. The external dose-rates were determined in this study using thick source alpha and beta counting on *Daybreak* and *Risø GM-25-5* measurement systems, respectively. The conversion factors provided by Guerin et al. (2011) were used, in addition to an alpha efficiency value (a-value) of 0.11 ± 0.03 after the measurements performed by Balescu and Lamothe (1993) (Table 2). The water contents for all samples (5 ± 2 %) are expressed as a percentage of the mass of dry sediment and informed by field measurements. Cosmic dose-rates were calculated in accordance with Prescott and Hutton (1994).

Feldspars form a solid-solution series, ranging from anorthite ($CaAl_2Si_2O_8$), to albite ($NaAlSi_3O_8$), to orthoclase ($KAlSi_3O_8$). Density separation is routinely used for luminescence dating to isolate the K-feldspar dominated fraction but this process can be difficult for some samples. Grain-to-grain variation in internal K-content is therefore an important factor to consider for single-grain dating of K-feldspars as the internal beta dose-rate originating from the K within the different grains may vary. Bulk K-contents of the density-separated K-feldspar fractions were measured for all samples in this study using 0.1 g sub-samples on a Risø GM-25-5 beta counter; the mean and standard deviation K-content measured for all the samples was 5.0 ± 1.0% K, and suggested that the geochemistry of grains in these samples was variable. LA-ICP-MS measurements performed on single grains of K-feldspar from samples LBA12OW1 and LBA12OW4 were then used to confirm that the internal K-contents of individual grains emitting detectable luminescence signals in these samples varied from 0 to 14% (Fig. S.1). The bedrock geology underlying the Northern Patagonian icefield includes both plutonic and basaltic rocks (Espinoza et al., 2010). The variability in internal K-contents measured for individual grains from this suite of samples is consistent with the mixture of perthitic and end member (i.e. K- or Na-rich) feldspar grains likely to have been sourced from the bedrock at Lago Buenos Aires.

Previous studies have shown a relationship between the single-grain D_e values and luminescence signal intensity measured in response to a fixed test dose for some well-bleached sedimentary samples, which contained feldspar grains of variable K-content (Reimann et al., 2012; Smedley, 2014). In these studies single-grain ages were calculated using only the D_e values for the grains emitting the brightest $pIRIR_{180}$ (Reimann et al., 2012) and $pIRIR_{225}$ signals (Smedley, 2014), and assumed internal K-contents of 12.5 ± 0.5% and 10 ± 2%, respectively. The ages determined were in good agreement with independent numerical age control and suggested that the range in internal K-contents of the K-feldspar grains was reduced by selecting the brightest grains. The LA-ICP-MS measurements performed on single grains of the density-separated K-feldspar fraction from samples in this study suggest that a similar approach is necessary to determine accurate ages (Fig. S.1). Therefore, only the D_e values determined for the brightest 20% of the grains for each sample were used to calculate ages, and an internal K-content of 10 ± 2% was assumed for dosimetry calculations (for more information see the supplementary materials provided in S.2).

5. Measurement of D_e values for luminescence dating

5.1. Equipment and measurement details

Samples were collected in either opaque tubes (2 mm thick plastic rim) that were hammered into the sedimentary section, or under an opaque cover sheet to prevent contact with direct sunlight during sampling. All samples were prepared under subdued red lighting conditions in the laboratory. The sedimentary samples were first treated with a 10% v.v. dilution of 37% HCl and with 20 v.v. of H_2O_2 to remove carbonates and organics, respectively. Dry sieving isolated the 180–210 μm or 180–250 μm diameter grains, and density separation using sodium polytungstate provided the <2.58 g cm^{-3} (K-feldspar-dominated) fractions. The K-feldspar grains were not etched in hydrofluoric acid because of concerns about anisotropic removal of the surface (Duller, 1992). Grains were mounted into 10 × 10 grids of 300 μm diameter holes in a 9.8 mm diameter aluminium single-grain disc for analysis.

All luminescence measurements were performed using a Risø TL/OSL DA-15 automated single-grain system equipped with a $^{90}Sr/^{90}Y$ beta source delivering ~0.04 Gy/s. The variability of the beta dose between grains for the source used in this study was found to be negligible with a relative standard error of ~2%. Each single-grain disc was located using the laser at room temperature to prevent annealing of the pIRIR signal during the time it takes to find the disc (Smedley and Duller, 2013). Stimulation was performed using an infra-red laser (830 nm) fitted with an RG-780 filter to remove any shorter wavelengths (Bøtter-Jensen et al., 2003), and a blue detection filter pack (BG-39, GG-400 and

Table 2
Dosimetry calculations for luminescence samples from Lago Buenos Aires. An internal K-content of 10 ± 2% was applied to determine the internal beta dose-rate for these samples (Smedley et al., 2012).

Sample	Depth (m)	Grainsize (μm)	K (%)	U (ppm)	Th (ppm)	Cosmic dose-rate (Gy/ka)	Alpha dose-rate (Gy/ka)	Beta dose-rate (Gy/ka)	Gamma dose-rate (Gy/ka)	External dose-rate (Gy/ka)	Internal dose-rate (Gy/ka)	Total dose-rate (Gy/ka)
LBA12OW3	1.0	180–250	2.72 ± 0.13	2.69 ± 0.30	7.64 ± 1.00	0.20 ± 0.01	0.16 ± 0.07	2.22 ± 0.45	1.27 ± 0.27	3.85 ± 0.53	0.65 ± 0.13	4.50 ± 0.55
LBA12OW5	0.5	180–250	1.83 ± 0.10	2.24 ± 0.22	7.34 ± 0.73	0.23 ± 0.01	0.14 ± 0.06	1.59 ± 0.33	1.00 ± 0.21	2.96 ± 0.39	0.65 ± 0.13	3.61 ± 0.42
LBA12RF1	1.8	180–250	1.83 ± 0.10	2.56 ± 0.24	5.99 ± 0.79	0.18 ± 0.01	0.14 ± 0.06	1.60 ± 0.33	1.05 ± 0.21	2.98 ± 0.39	0.65 ± 0.13	3.63 ± 0.42
LBA12OW1	1.5	180–210	1.83 ± 0.10	2.13 ± 0.25	6.74 ± 0.83	0.19 ± 0.01	0.13 ± 0.06	1.56 ± 0.32	0.96 ± 0.21	2.85 ± 0.39	0.58 ± 0.12	3.42 ± 0.40
LBA12OW4	2.0	180–210	1.80 ± 0.10	2.43 ± 0.25	6.54 ± 0.82	0.18 ± 0.01	0.14 ± 0.06	1.58 ± 0.32	0.98 ± 0.21	2.87 ± 0.39	0.58 ± 0.12	3.45 ± 0.41
LBA12OW2	1.0	180–210	1.87 ± 0.10	2.32 ± 0.25	6.75 ± 0.84	0.20 ± 0.01	0.14 ± 0.06	1.61 ± 0.33	0.99 ± 0.21	2.95 ± 0.40	0.58 ± 0.12	3.52 ± 0.42
LBA12F4-2	8.0	180–250	2.35 ± 0.11	1.99 ± 0.24	6.37 ± 0.80	0.09 ± 0.01	0.13 ± 0.06	1.87 ± 0.38	1.00 ± 0.21	3.09 ± 0.44	0.65 ± 0.13	3.75 ± 0.46
LBA12F4-3	8.0	180–210	2.06 ± 0.10	2.30 ± 0.23	5.42 ± 0.80	0.09 ± 0.01	0.13 ± 0.06	1.70 ± 0.35	0.98 ± 0.21	2.90 ± 0.41	0.58 ± 0.12	3.47 ± 0.43
LBA12F4-1	6.0	180–250	1.83 ± 0.10	2.15 ± 0.26	7.35 ± 0.87	0.11 ± 0.01	0.14 ± 0.06	1.58 ± 0.32	0.97 ± 0.19	2.80 ± 0.38	0.65 ± 0.13	3.45 ± 0.40
LBA12M1-1	1.0	180–210	1.60 ± 0.11	2.23 ± 0.23	5.49 ± 0.76	0.20 ± 0.01	0.13 ± 0.06	1.40 ± 0.29	0.86 ± 0.19	2.58 ± 0.35	0.58 ± 0.12	3.16 ± 0.37
LBA12M1-2	2.0	180–210	2.16 ± 0.10	1.93 ± 0.26	7.23 ± 0.86	0.18 ± 0.01	0.13 ± 0.06	1.76 ± 0.36	1.04 ± 0.22	3.11 ± 0.43	0.58 ± 0.12	3.69 ± 0.44
LBA12M3	3.5	180–250	1.75 ± 0.09	2.01 ± 0.22	5.93 ± 0.73	0.14 ± 0.01	0.12 ± 0.06	1.48 ± 0.30	0.89 ± 0.19	2.64 ± 0.36	0.65 ± 0.13	3.30 ± 0.39
LBA12D2-1	2.0	180–250	1.90 ± 0.10	2.14 ± 0.25	6.77 ± 0.83	0.18 ± 0.01	0.14 ± 0.06	1.61 ± 0.33	0.98 ± 0.21	2.91 ± 0.40	0.65 ± 0.13	3.56 ± 0.42

Corning 7-59) was placed in front of the photomultiplier tube. The signal was recorded for a total of 1.7 s, and the IRSL signal was summed over the first 0.3 s (10 channels) of stimulation and the background calculated from the final 0.6 s (20 channels). The instrument reproducibility of the single-grain measurement system was measured using the pIRIR signal (2.5%; Smedley and Duller, 2013) and incorporated into the calculation of the D_e values.

The single aliquot regenerative dose (SAR) protocol using the $pIRIR_{225}$ signal in this study is shown in Table 3. Five screening criteria were applied to the resulting data throughout the analyses unless otherwise specified. Grains were only accepted if (1) the response to the test dose was greater than three sigma above the background, (2) the test dose uncertainty was less than 10%, (3) the recycling ratio (including the associated uncertainties) was within the range of ratios 0.9 to 1.1, (4) recuperation was less than 5% of the response from the largest regenerative dose (96 Gy) and (5) the single-grain D_e values were not part of a population of very low doses that were identified by the finite mixture model (FMM) to be inconsistent with the geological context of the sample (e.g. Smedley, 2014). A luminescence age was then determined by dividing the D_e value by the environmental dose-rate that the grains were exposed to throughout burial.

5.2. Assessing the $pIRIR_{225}$ signal for single-grain dating

5.2.1. Optical bleaching

For luminescence dating in an environment where the opportunity for bleaching is limited (e.g. glacial settings) it is important to consider how rapidly the luminescence signal used for dating bleaches in response to optical stimulation (e.g. sunlight). Although the pIRIR signal may be more stable over time than the IR_{50} signal, several multiple-grain studies of coarse-grained K-feldspar have demonstrated that the pIRIR signal bleaches more slowly in response to optical stimulation than the IR_{50} signal (Buylaert et al., 2012; Murray et al., 2012), which in turn bleaches more slowly than the OSL signal from quartz (Godfrey-Smith et al., 1988). If the signal used for luminescence dating bleaches more slowly in response to sunlight in nature, it is more likely that larger residual doses are incorporated into the D_e values determined in the laboratory. This has led some authors to prefer the IR_{50} signal for single-grain dating of K-feldspar in environments where there is limited exposure to sunlight instead of the pIRIR signal (Alexanderson and Murray, 2012; Blombin et al., 2012). However, Smedley et al. (2015) have demonstrated that the $pIRIR_{225}$ signal bleaches more rapidly than the $pIRIR_{290}$ signal for individual grains of K-feldspar. The authors also performed short laboratory bleaching experiments on two well-bleached samples and one partially-bleached sample with independent age control to demonstrate that the bleaching rates of the $pIRIR_{225}$ signal for individual grains of K-feldspar did not have a dominant control on the single-grain D_e distributions. Therefore, the $pIRIR_{225}$ signal was preferred for single-grain dating of K-feldspar in this study.

Table 3
Experimental details for the single-aliquot regenerative dose (SAR) pIRIR experiments performed throughout this study. Test-doses of 52 Gy were used for all the experiments in this study except for the measurements to determine residual D_e values, where test-doses of 4 Gy were used.

Step	Treatment
1	Dose
2	Preheat 250 °C for 60 s
3	IR LEDs 100 s at 60 °C
4	SG IRSL 2 s at 225 °C
5	Test dose (52 Gy or 4 Gy)
6	Preheat 250 °C for 60 s
7	IR LEDs 100 s at 60 °C
8	SG IRSL 2 s at 225 °C
9	IR LEDs 100 s at 290 °C

5.2.2. Recovering a laboratory dose

Dose-recovery and residual-dose experiments were performed on sample LBA12F4-2 to assess the suitability of the measurement protocol using the $pIRIR_{225}$ signal. The residual D_e value measured after a given dose of 50 Gy and an 8 h bleach in the solar simulator (SOL2) was 2.7 ± 0.4 Gy (n = 25 grains). The residual-subtracted dose-recovery ratio determined was 1.12 ± 0.07 and demonstrated that the measurement conditions were appropriate for dating these samples. The overdispersion value calculated for dose-recovery experiments of sample LBA12F4-2 was 21 ± 1% and quantifies the minimum amount of scatter beyond measurement uncertainties that can be incorporated into a single-grain D_e distribution from measurements performed in the laboratory.

5.2.3. Anomalous fading

Fading measurements are typically performed for luminescence dating of K-feldspar grains to determine whether fading correction of the luminescence signal is necessary to provide accurate ages. Measuring accurate fading rates (termed g-values) from single grains of K-feldspar is difficult due to the low sensitivity of the IRSL signals from some of the grains. Therefore, fading measurements were performed in this study on a large suite of medium aliquots to determine the best estimate of the fading rate for this suite of samples. Five multiple-grain aliquots from 12 of the 13 samples (n = 60 aliquots) were used to determine g-values. Fading rates were determined for both the $pIRIR_{225}$ signal and the less stable IR_{60} signal built into the $pIRIR_{225}$ protocol (termed the $IR_{60/225}$ signal), and were normalised to two days (Auclair et al., 2003). The g-values measured using the $IR_{60/225}$ and $pIRIR_{225}$ signals formed a normal distribution around a central value (Fig. 5a) so the weighted means and standard errors were calculated for each of the two datasets to provide the best estimate of fading. The g-values determined were 4.1 ± 0.1%/decade ($IR_{60/225}$ signal) and 1.0 ± 0.1%/decade ($pIRIR_{225}$ signal). The fading rate determined using the $pIRIR_{225}$ signal for this suite of samples (1.0 ± 0.1%/decade) was consistent with fading rates typically measured using the $pIRIR_{225}$ signal of other samples (e.g. Roberts, 2012; Trauerstein et al., 2014), and also similar to g-values measured for the OSL signal of quartz (e.g. Buylaert et al., 2012; Thiel et al., 2011). Given that luminescence dating of quartz is not routinely corrected for fading, the measurement of g-values for K-feldspar that are consistent with quartz fading rates implies that this magnitude of effect is negligible, and may just be an artefact of the measurement procedure (e.g. Buylaert et al., 2012; Thiel et al., 2011). Therefore, fading correction of the $pIRIR_{225}$ signal was not performed in this study.

5.3. Selection of statistical age models

Overdispersion values calculated for single-grain D_e distributions provide an estimate of the amount of scatter in a dataset beyond that of measurement uncertainties. This information can often be used in conjunction with the knowledge of the geological context of a sample to determine which statistical model is appropriate for providing an age (Galbraith and Roberts, 2012). The range of overdispersion values from 26 ± 1% (sample LBA12OW1) to 80 ± 1% (sample LBA12F4-1) for the single-grain D_e values of samples in this study suggests that the D_e distributions for some of the samples were more scattered than others (Table 1). Given that the samples had similar geochemical and depositional contexts it is likely that the extent of bleaching upon deposition in this glaciated

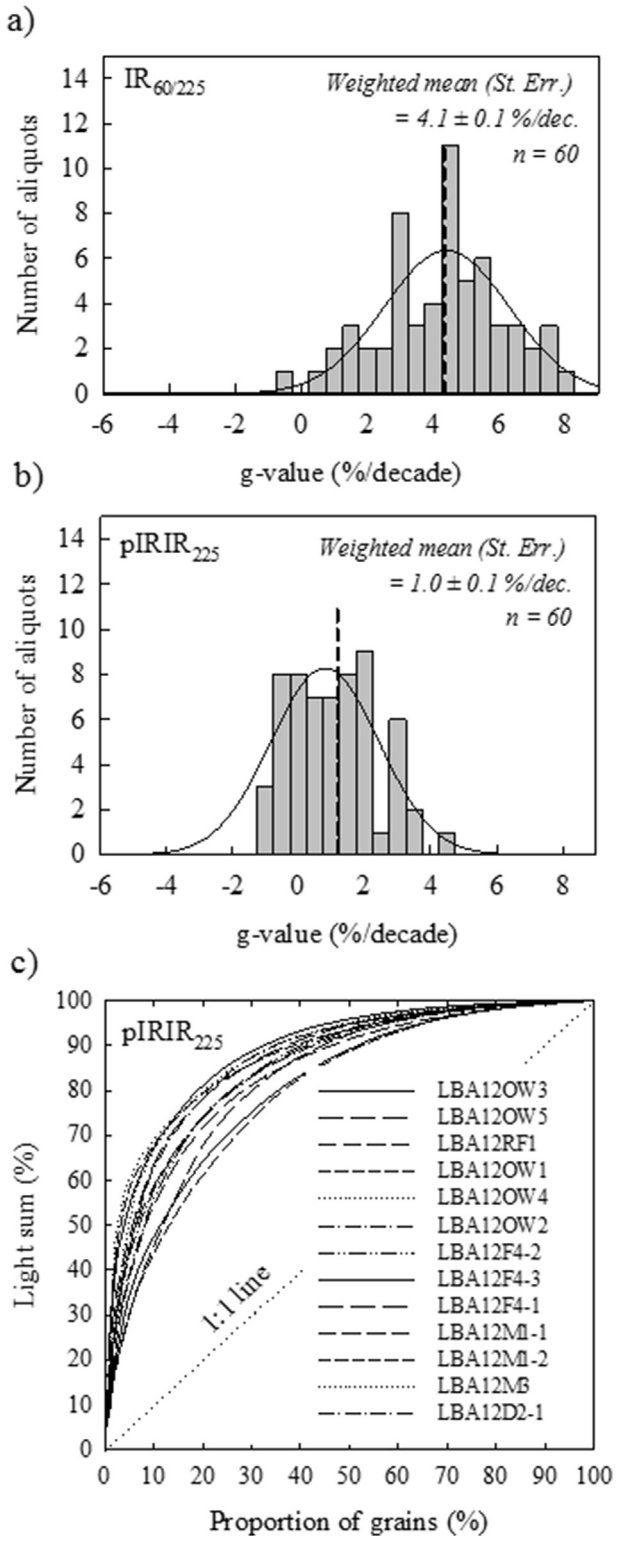

Fig. 5. Histograms of the fading rates measured for the samples using the $IR_{60/225}$ (a) and $pIRIR_{225}$ (b) signals. A Gaussian fit has been applied to these data (solid line). Repeated L_x/T_x measurements were performed using the $IR_{60/225}$ and $pIRIR_{225}$ signals after progressively longer storage times (inserted between steps 2 and 3 of Table 3), from a prompt measurement after ~0.2 h to the maximum delay time of ~680 h i.e. ~1 month. Note that fading measurements were not performed on samples LBA12M1-1 and LBA12M1-2. The distribution of the signal-intensity emitted from single-grain K-feldspars for the suite of glacial samples extracted from Lago Buenos Aires are also shown (c). Data are plotted as the proportion of the total light sum that originates from the specified percentage of the brightest grains.

environment was the dominant controlling factor on the scatter in the D_e distributions. Those samples with lower overdispersion values were likely to have been well bleached upon deposition and those with higher overdispersion values were likely to have been partially bleached. Applying the Central Age Model (CAM) is most appropriate to determine accurate ages for well-bleached samples, whereas the Minimum Age Model (MAM) is most appropriate for samples that were partially bleached upon deposition (Galbraith and Roberts, 2012). However, it is important to consider that other factors, such as luminescence characteristics, microdosimetry and post-depositional processes can cause scatter in D_e distributions.

Arnold and Roberts (2009) summarise the overdispersion values for single-grain D_e distributions determined for quartz from a range of samples thought to have been well bleached upon deposition. The overdispersion values ranged from 0 to 40%, with a mean and standard deviation of 20 ± 9%. For the samples in this study it is hypothesised that a threshold of 50% can be used to differentiate between well-bleached and partially-bleached samples from Lago Buenos Aires. To test this hypothesis the luminescence ages determined for four samples that could be directly linked to specific moraine ridges by the geomorphology were compared to the cosmogenic isotope ages. Two of the samples had overdispersion values ≤50% (samples LBA12OW3 and LBA12OW1), and two had values >50% (samples LBA12OW4 and LBA12OW2). Examples of the sedimentology and single-grain D_e values for one of the samples with an overdispersion value of ≤50% (LBA12OW1; Fig. 6a, c) and >50% (LBA12OW2; Fig. 6b, d) are shown in Fig. 6.

The CAM ages calculated for the four samples are compared to the cosmogenic isotope ages of the moraines in Fig. 6e to assess the validity of the suggested overdispersion threshold used for age model selection. The two samples with overdispersion values of ≤50% had CAM ages in agreement with the cosmogenic isotope ages, and the CAM ages for those samples with overdispersion values of >50% overestimated the cosmogenic isotope ages. The agreement between the CAM ages and cosmogenic isotope ages for the samples with overdispersion values ≤ 50% confirms that these samples were likely to have been well bleached upon deposition. To calculate accurate ages with the MAM, the amount of scatter characteristic of a well-bleached sample from the natural environment under investigation (σ_b) needs to be quantified. Therefore, the mean of the overdispersion values determined from the two samples determined to have been well bleached upon deposition (~30%) was used to define the σ_b value for the MAM in this study; this overdispersion value was similar to the 20 ± 9% determined for single grains of quartz (Arnold and Roberts, 2009). The MAM was then used to calculate ages for the samples with overdispersion values >50% and the ages calculated agreed with the cosmogenic isotope ages (Fig. 6f). Based on the nature of the single-grain D_e distributions and the depositional contexts of the samples, an overdispersion threshold of 50% was used for age model selection for all the samples in this study.

The sedimentology of sample LBA12OW1 (overdispersion ≤50%; Fig. 6a) was well sorted and characteristic of less energetic depositional environments with greater opportunity for bleaching upon deposition than a more energetic depositional environment. In contrast, the sediment of sample LBA12OW2 (overdispersion >50%; Fig. 6b) was poorly-sorted and characteristic of higher-energy depositional environments, typical of more turbulent water columns, where there is less opportunity for bleaching upon deposition. These observations are consistent with research assessing the relationship between sedimentary lithofacies and the potential for bleaching in a glacial environment (Fuchs and Owen, 2008; Thrasher et al., 2009a,b).

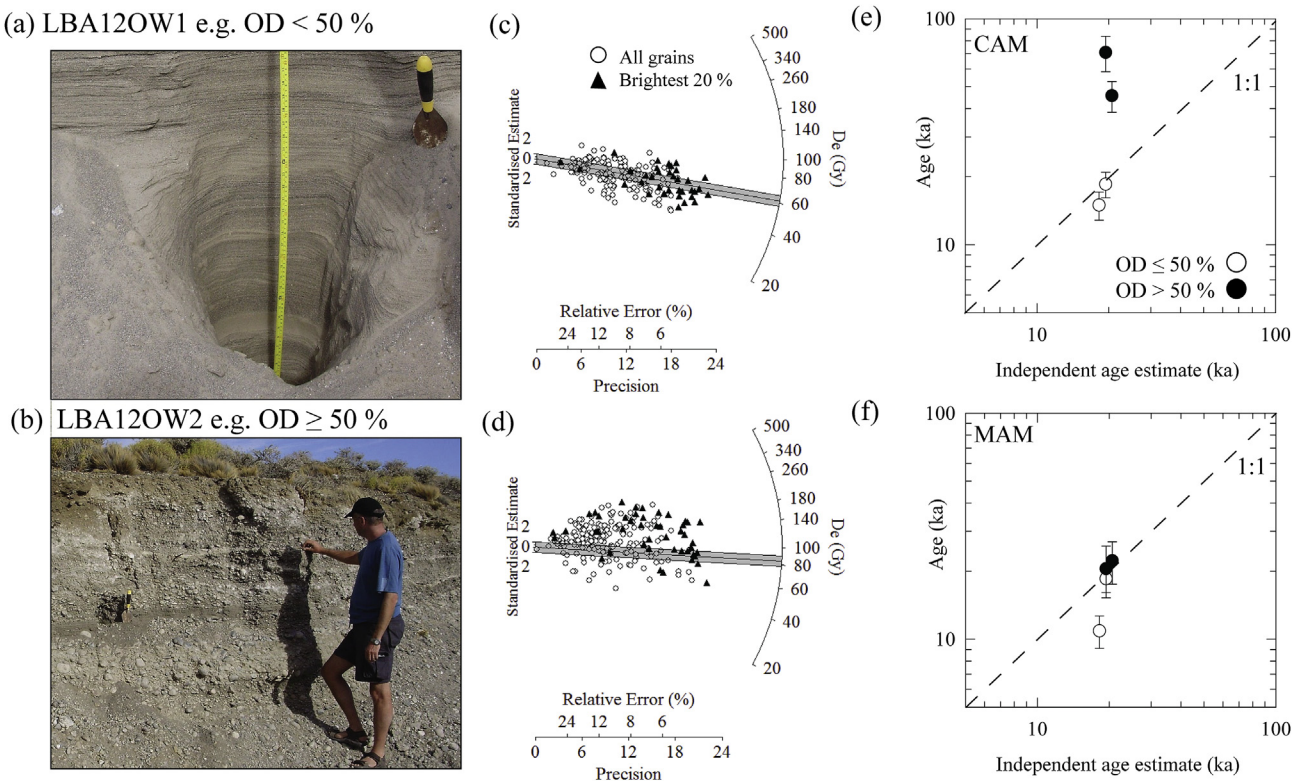

Fig. 6. Examples of samples that determined overdispersion values of ≤50% (LBA12OW1) and >50% (LBA12OW2). Photographs of the sedimentary sections sampled for LBA12OW1 (a) and LBA12OW2 (b) are shown in addition to the radial plots presenting the D_e values measured for each sample in (c) and (d), respectively. The radial plots present both the brightest 20% of the grains and all the grains measured. The grey bars show the CAM (c) and MAM (d) D_e values measured from only the brightest 20% of grains. Luminescence ages calculated when applying the CAM (e) and MAM (f) for four samples are plotted against independent age control provided by cosmogenic isotope dating.

6. Results

The total number of grains analysed to determine D_e values for each sample ranged from 600 to 1900 (see Table S.2 for details). Fig. 5c presents cumulative light sum plots (after Duller, 2000) for all the samples in this study. The number of grains passing the screening criteria and providing D_e values ranged from 6.4 to 30.0% of the total grains analysed, and the brightest 20% of the grains for each sample accounted for between only 1.3% and 6.0% of the total grains analysed (Table 1; Fig. S.4). The single-grain ages determined for all of the samples in this study are shown in Fig. 7 in relation to the cosmogenic isotope ages provided for the moraine ridges (Kaplan et al., 2011) and the $^{40}Ar/^{39}Ar$ age provided for the Cerro Volcán lava flow (Singer et al., 2004). The luminescence age of each sample is also shown in Figs. 3 and 4. The Fenix and Moreno samples can be clearly differentiated by the luminescence ages into different glacial periods, which is consistent with the pre-existing chronology.

6.1. Luminescence ages for the Fenix moraines

The luminescence ages for the glaciofluvial sediments associated with the Menucos and Fenix moraines are in chronological order in accordance with the sedimentological and geomorphological context of each sample, e.g. sample LBA12OW3 (14.7 ± 2.1 ka) is the youngest and sample LBA12F4-2 (30.8 ± 5.7 ka) is the oldest. The luminescence ages are also in good agreement with the pre-existing chronology provided for the Fenix moraines. For those samples where the geomorphological and sedimentological context was difficult to interpret (samples LBA12OW5, LBA12RF1, LBA12F4-1 and LBA12F4-2), the use of the geomorphology, elevation profile and conceptual model suggest that the luminescence ages were feasible in the context of the surrounding chronological dataset.

The luminescence age of LBA12OW5 (20.2 ± 4.5 ka) suggests that this sample was deposited at a similar time to the Fenix I and Fenix II moraine ridges. This is feasible because sample LBA12OW5 was taken from a relic glaciofluvial terrace (elevated ~415 m) of the central meltwater channel draining through the valley (Fig. 3b), which was truncated by younger meltwater drainage events since formation. Also, the luminescence age provided for sample LBA12F4-1 suggests that these glaciofluvial sediments were deposited at a similar time to sample LBA12OW2 and the Fenix III moraine ridge, but within uncertainties of the cosmogenic isotope ages for the Fenix IV and V moraines. This is feasible as the sample was taken from the upper part of the sedimentary sequence at this site. The luminescence age for sample LBA12F4-2 is older than sample LBA12F4-1 and is therefore internally consistent with the sedimentology of these sections. The age of sample LBA12F4-2 (30.8 ± 5.7 ka) is, however, at the upper limit of agreement with the cosmogenic ages for the Fenix IV and V moraines. The age of sample LBA12F4-2, in addition to the age of sample LBA12RF1 (34.0 ± 6.1 ka), suggests that glaciofluvial sediments have been preserved at Lago Buenos Aires from an earlier glacial advance (or advances) that has later been overrun by the glacial advances of the Fenix IV and V moraine ridges. The conceptual model (Fig. 2) demonstrates that preservation of outwash sediments from an earlier glaciation is feasible as these sediments were taken from units that were either deposited at lower elevations in the sedimentary sequence or have been thrust up from lower elevations by post- or syn-depositional processes.

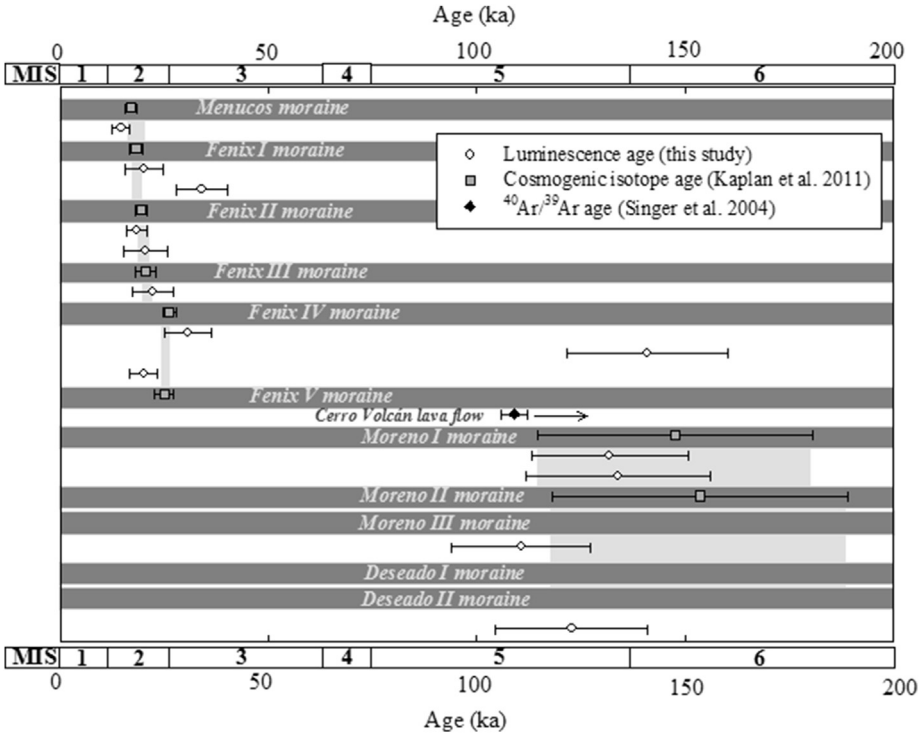

Fig. 7. Comparison of the luminescence ages provided in this study with the cosmogenic isotope ages (Kaplan et al., 2004; Douglass et al., 2006) that were re-calculated by Kaplan et al. (2011). The ages are shown as weighted means and standard deviations, which do not include those ages identified as outliers in the original publication. Also shown is an $^{40}Ar/^{39}Ar$ age (Singer et al., 2004) for the Cerro Volcán lava flow constraining the deposition of the moraine ridges at Lago Buenos Aires.

6.2. Luminescence ages for the Moreno and Deseado moraines

The fundamental principles of luminescence dating require that there is an upper age limit to the dating technique; this limit is dependent upon factors inherent to the sample, mineral type and signal used for analysis. The accumulation of energy from ionizing radiation within the crystalline structure of a mineral grain can reach saturation at larger doses and therefore can complicate luminescence dating of older samples. In luminescence dating saturation can be determined from the dose-response curve, and a prudent limit above which D_e estimation may be unreliable has been suggested to be two times D_0 (the characteristic dose in an exponential fit) by Wintle and Murray (2006). Duller (2012) has demonstrated that single grains of quartz have different saturation limits; this variability may impact upon the single-grain D_e distributions for older samples, and so it is important that the saturation limits of the K-feldspar grains used for dating older samples in this study are investigated.

Single-grain D_0 values were calculated for the proglacial samples associated with the Moreno and Deseado moraines to investigate the grain-to-grain variability in D_0 values of K-feldspar grains. Means and standard deviations were calculated for the $2D_0$ values determined for the grains used to determine D_e values (i.e. the brightest 20% of the grains); the results ranged from 489 ± 161 Gy to 651 ± 252 Gy. There was a large amount of variability in the $2D_0$ values measured for individual grains. For example, the $2D_0$ values determined for single grains from sample LBA12D2-1 ranged from 182 to 1423 Gy. Based on the underlying $^{40}Ar/^{39}Ar$ age of the Cerro Volcán lava flow, the Deseado II moraine and the associated glaciofluvial sediment (sample LBA12D2-1) must be >109 ± 3 ka. Therefore, the expected D_e value for sample LBA12D2-1 is >390 Gy, according to the dose-rate of 3.56 ± 0.42 Gy/ka determined for this sample (Table 2). This implies that some of the grains analysed were approaching saturation for sample LBA12D2-1 as the grains were characterised by $2D_0$ values as low as 182 Gy, but a large proportion of grains had $2D_0$ values in excess of the expected D_e value. In practise the luminescence signals of grains that were approaching saturation are unlikely to influence the D_e distribution as the L_n/T_n ratios cannot be interpolated on to a dose-response curve (Duller, 2012). Moreover, large and asymmetric uncertainties are determined for grains at the limit of saturation, which means the statistical age models will weight the age towards those D_e values more precisely known i.e. those not approaching saturation. Thus, luminescence dating of samples associated with the Moreno and Deseado moraines is not restricted by saturation of the $pIRIR_{225}$ signal.

The overdispersion values for the suite of samples related to the Fenix moraines ranged from 26 to 80%, whereas the overdispersion values for the Moreno and Deseado samples ranged from only 38 to 52%. The smaller range in overdispersion values potentially suggests that the proportion of scatter in these D_e distributions caused by partial bleaching upon deposition (which will be similar to that experienced by outwash associated with the Fenix moraines) accounts for a smaller proportion of the overall doses. Residual signals caused by the effects of partial bleaching have previously been reported to account for a larger proportion of the burial dose for young fluvial sediments in comparison to older samples (Jain et al., 2004). The reduced influence of partial bleaching on the samples associated with the Moreno and Deseado moraines suggests that the CAM can be applied to determine accurate ages for these sediments; this is supported by the excellent agreement between luminescence ages determined for the Moreno and Deseado moraines, in addition to the cosmogenic isotope ages.

The two luminescence ages determined for the Moreno I moraine ridge (LBA12M1-1 – 132 ± 19 ka; LBA12M1-2 – 134 ± 22 ka) were within ±1 σ of one another and the cosmogenic

isotope age determined for the Moreno I moraine ridge (~150 ± 35 ka). The luminescence age determined for the ponded feature incorporated into the Moreno III moraine ridge (111 ± 17 ka) was within uncertainties of the luminescence and cosmogenic isotope ages determined for the Moreno I and II moraine ridges. However, the age was at a lower limit of the age interval provided for the Moreno I and II moraines when considering the uncertainties, and may suggest that the grains within the ponded feature were deposited after the glacial advance. Currently, there are no cosmogenic isotope ages constraining the deposition of the Deseado moraine ridges. The new luminescence age provided for sample LBA12D2-1 in this study suggests that the outwash plain associated with the Deseado II moraine ridge was deposited 123 ± 18 ka, and therefore the outwash associated with the Deseado II moraine was deposited during MIS 6 at a similar time to the Moreno moraines.

7. Discussion

The new luminescence ages provided in this study (Fig. 7) contribute towards the continued advancement and refinement of the luminescence dating technique in glaciated environments, but the ages also provide insights into the glacial history preserved at Lago Buenos Aires since MIS 6.

7.1. Moreno and Deseado moraines at Lago Buenos Aires

Ages provided for the Moreno and Deseado moraines in this study using luminescence and cosmogenic isotope dating suggest that sediments have been preserved at Lago Buenos Aires from glacial advances from ~110 ± 20 ka to 150 ± 30 ka. Palaeoenvironmental records linked with Patagonia suggest that it is possible for glacial advances to have occurred during MIS 6. Dust in the EPICA Dome C ice core (75 °S, 123 °E) which has been geochemically fingerprinted to Patagonia recorded high concentrations during MIS 6, indicating that glacial conditions likely prevailed at this time (Lambert et al., 2008). Also, the $\delta^{18}O$ record indicates that global ice volumes were increased during MIS 6 (Imbrie et al., 1984).

It is interesting to observe that glacial advances during MIS 6 have been preserved at Lago Buenos Aires, but there are currently no sediments recorded from MIS 4, which is a time with similar palaeoenvironmental records to MIS 6 (i.e. increased global ice volumes). In order to further define the glacial record and provide comparisons to the palaeoenvironmental record, more age constraints for the timing of glacial advances prior to MIS 2 and 3 are required from across Patagonia and the Southern Hemisphere.

7.2. Fenix moraines at Lago Buenos Aires

The luminescence ages for the deposition of outwash sediments associated with the Fenix moraines at Lago Buenos Aires (Fig. 8e) appear to fall into two groups (grey shading in Fig. 8): earlier advances during MIS 3 and later advances during MIS 2 (referred to as phases MIS 2a and MIS 2b in Fig. 8).

7.2.1. Glacial advances: MIS 3

The oldest Fenix moraine ridges preserved at Lago Buenos Aires are the Fenix IV (26.2 ± 1.6 ka) and Fenix V (25.0 ± 2.3 ka) moraines (Kaplan et al., 2011), but luminescence dating for glaciofluvial sediments suggests that outwash plains were deposited at Lago Buenos Aires as early as 30.8 ± 5.7 ka (LBA12F4-2) and 34.0 ± 6.1 ka (LBA12RF1) during MIS 3 (Fig. 8e). The older outwash plains were deposited at lower elevations in the sedimentary sequence, which may have allowed them to be preserved when the more prominent moraine ridges were destroyed during subsequent glacial advances.

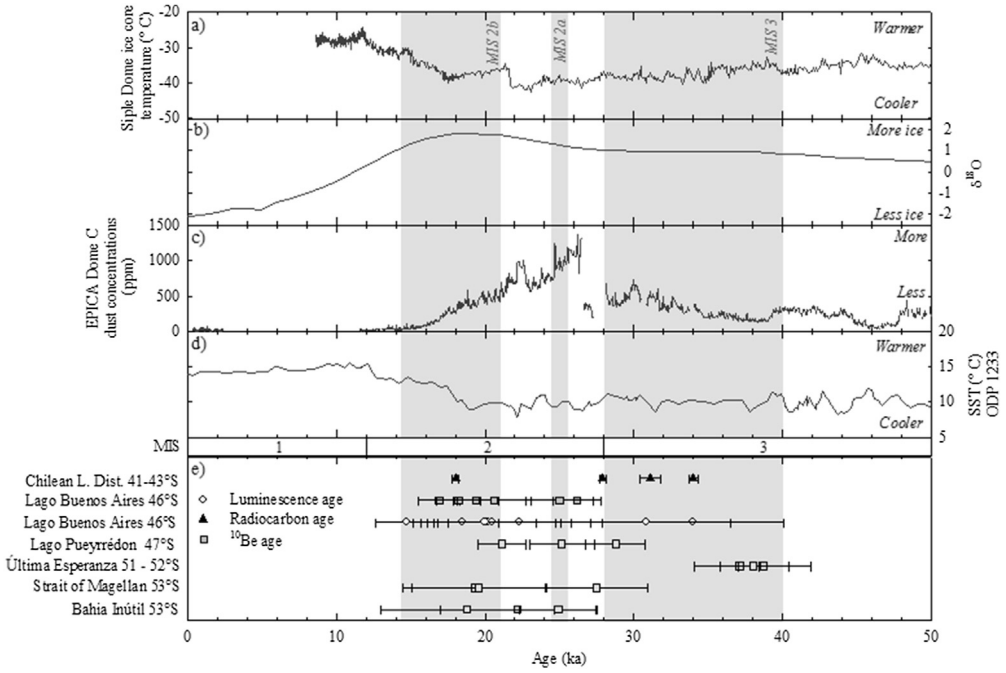

Fig. 8. Palaeoenvironmental records for the last 50 ka. (a) Temperature estimated from Siple Dome Ice Core, West Antarctica (81 °S, 148 °W), ice core hydrogen isotope (deuterium, δD) data, with age model correlated to the GISP2 ice core time scale using methane and $\delta^{18}O$ from 9 to 57 Ka BP (Brook et al., 2005). (b) Global $\delta^{18}O$ records developed by the SPECMAP project (Imbrie et al., 1984), (c) Dust concentrations from the EPICA Dome C ice core (75 °S, 123 °E) (Lambert et al., 2008). (d) Sea surface temperature records from ODP core 1233 (41 °S, 74°W) (Kaiser et al., 2005). (e) Cosmogenic isotope ages (Douglass et al., 2006; Kaplan et al., 2004, 2005) re-calculated by Kaplan et al. (2011) and luminescence ages (this study) for Lago Buenos Aires. Also shown are: (1) radiocarbon ages from the Chilean Lake District (Denton et al., 1999; re-calibrated by Putnam et al., 2013); (2) cosmogenic isotope ages from Lago Pueyrrédon (Hein et al., 2010), the Strait of Magellan and Bahia Inútil (Kaplan et al., 2008; McCulloch et al., 2005) that were all re-calculated by Kaplan et al. (2011); (3) cosmogenic isotope ages from the Última Esperanza region, Chile (Sagredo et al., 2011).

Evidence for glacial advances during MIS 3 has also been recorded by radiocarbon dating of plant macrofossils that were overrun by ice in the Chilean Lake District (Fig. 8e; Denton et al., 1999). Cosmogenic isotope dating of moraine boulders (37.1 ± 1.3 ka, 38.7 ± 1.7 ka and 38.0 ± 3.9 ka) in the Última Esperanza region has also identified moraine ridges preserved from glacial advances during MIS 3 (Sagredo et al., 2011). Finally, Darvill et al. (2015) used cosmogenic nuclide dating of outwash sediments to determine glacial limits from MIS 3 for the Bahia Inútil lobe in southern Patagonia, which were more extensive than the MIS 2 limits. No other published evidence of glacial advances at this time exists from Patagonia, but a trend of increasing dust levels in the EPICA Dome C ice core (Fig. 8c) and low sea surface temperatures (SST) off the west coast of Chile (Fig. 8c) are seen between ~31 ka and ~37 ka; this may be related to an increase in ice extent at Lago Buenos Aires.

The timings of earlier phases of glaciation that occurred during MIS 3 in the Chilean Lake District, at Lago Buenos Aires and at Bahia Inútil suggest that these phases occurred across ~12° of latitude in Patagonia. However, summer insolation in the Southern Hemisphere was high ~31–37 ka (Berger and Loutre, 1991) and temperatures in West Antarctica (81 °S) were warmer than during full glacial conditions ~18–25 ka (Fig. 8a; Brook et al., 2005). The conditions recorded in the palaeoenvironmental archive therefore question why glacial advances ~31–37 ka (MIS 3) in Patagonia reached similar lateral extents to the advances during the LGM of MIS 2 (~18–25 ka).

7.2.2. Glacial advances: MIS 2

Cosmogenic isotope ages of the Fenix IV (26.2 ± 1.6 ka) and Fenix V (25.0 ± 2.3 ka) moraine ridges records the major glacial advances at Lago Buenos Aires during MIS 2 (Kaplan et al., 2011). However, the timing of these major advances occurred later at Lago Buenos Aires than is suggested by the evidence preserved elsewhere in Patagonia (Fig. 8e). The major glacial advances at Lago Pueyrrédon (28–30 ka; Hein et al., 2010; Kaplan et al., 2011), in the Chilean Lake District (27 cal. ka; Denton et al., 1999) and in the Strait of Magellan and Bahia Inútil (~27–29 ka; McCulloch et al., 2005; Kaplan et al., 2008, 2011) were all consistent and occurred ~2 ka prior to the major glacial advances at Lago Buenos Aires (~25 ka). Moraine ridges that were deposited at a similar time to Fenix IV and V at Lago Buenos Aires (~25 ka) are preserved within the limits of larger advances occurring ~27 ka at Lago Pueyrrédon (Hein et al., 2010; Kaplan et al., 2011), Bahia Inútil (Kaplan et al., 2008; McCulloch et al., 2005) and in the Chilean Lake District (Denton et al., 1999). Moraine deposition in Patagonia ~25 ka (Fig. 8 grey shading; MIS 2a) occurs at the same time as cooler SST off the west coast of Chile (Fig. 8d) and high concentration of dust in the EPICA Dome C ice core (Fig. 8c).

Multiple glacial advances have then been recorded at Lago Buenos Aires from ~18 to 23 ka by the Fenix I to III moraine ridges. Fig. 8e shows that the glacial advances at Lago Buenos Aires from ~18 to 23 ka are in phase with records provided from across Patagonia (41–53 °S). The Rio Blanco moraine limit 3 in the Lago Pueyrrédon valley records an advance from cosmogenic isotope dating between 20 and 22 ka, respectively (Hein et al., 2010; Kaplan et al., 2011). Glacial advances are also recorded in the Strait of Magellan (~19–20 ka) and Bahia Inútil (~19–25 ka) (Kaplan et al., 2008; McCulloch et al., 2005), which were deposited at similar times to the moraine ridges in the Chilean Lake District at ~19, 21 and 25 cal. ka BP (Denton et al., 1999). The palaeoenvironmental record reports that environmental conditions in the Southern Hemisphere fluctuated from ~18 to 23 ka (Fig. 8 grey shading; MIS 2b) according to the dust concentrations in the EPICA Dome C ice core (Fig. 8c) and minor fluctuations in SST recorded in the ODP core off the coast of Chile (Fig. 8d). Also, temperatures recorded in the Siple Dome ice core in western Antarctica (Fig. 8a) cooled from ~23 ka into a distinctly cooler period occurring ~22–23 ka, which was followed by a rapid increase in temperature ~21 ka, and the global ice volume increased (Fig. 8b). The similar timings of events in the palaeoenvironmental record and glacial advances across Patagonia suggest that fluctuations in the extent of the Patagonian Ice Sheet were sensitive to changes in climate throughout the LGM.

The glacial record from Patagonia suggests that the final glacial advance occurred ~18 ka, which corresponds to the deposition of the Fenix I moraine ridge. Cosmogenic isotope ages for the final glacial advance preserved at Lago Pueyrrédon suggest that it occurred ~19–20 ka (Hein et al., 2010; Kaplan et al., 2011) where lake formation then persisted from 15 to 17 ka (Mercer, 1976; Mercer and Sutter, 1982; Turner et al., 2005). This is consistent with cosmogenic isotope dating of former ice limits around Cerro Tamango, Cerro Oportus and Sierra Colorado at Lago Pueyrrédon, where the ice lobe had retreated to within 10–15 km of the present-day extent from 15.6 to 19 ka, with a still-stand or advance occurring ~16.9 ka (Boex et al., 2013). Similarly, the final extent of glaciation is recorded at 18 cal. ka in the Chilean Lake District (Denton et al., 1999) and ~17 cal. ka in the Strait of Magellan and Bahia Inútil (McCulloch et al., 2005; Kaplan et al., 2008, 2011). The lacustrine sediments preserved in the sedimentary record at Lago Buenos Aires indicate that a lake formed from ~18 ka. A later glacial advance then deposited the Menucos moraine at 16.9 ± 1.4 ka (Kaplan et al., 2011) similar to the still-stand or advance reported at Lago Pueyrrédon (Boex et al., 2013). Glacial conditions must then have persisted for the glaciofluvial sediments sampled by LBA12OW3 (14.7 ± 2.1 ka) to have been deposited. The sedimentary record at Lago Buenos Aires therefore suggests that glacial advances potentially occurred here later than in the rest of Patagonia (i.e. at Lago Pueyrrédon, in the Strait of Magellan and at Bahia Inútil).

Palaeoenvironmental records suggest that glacial conditions could have prevailed across Patagonia up to ~15 ka (Fig. 8). Although the temperature records in West Antarctica (Fig. 8a) and the SST in the ODP core off the coast of Chile had begun to increase from ~18 ka, the conditions were still commensurate with large ice volumes present in Patagonia up to ~15 ka: (1) the $\delta^{18}O$ records indicate that the global ice volume remained extensive until ~15 ka; (2) the dust concentrations in the EPICA Dome C ice core were still decreasing from the MIS 2 maximum; and (3) the SST were increasing, but did not reach significantly warmer temperatures than the MIS 2 maximum until after ~15 ka. Therefore, it is plausible that ice persisted at Lago Buenos Aires until ~15 ± 2 ka but evidence for this has not been preserved (or discovered) elsewhere. After ~15 ± 2 ka the ice front at Lago Buenos Aires retreated into the mountains and re-stabilised during the Younger Dryas, ~100 km from the LGM position, and ~50 km from the present ice front (Glasser et al., 2012).

7.3. Factors controlling glacial advances across Patagonia

The differences in timings of glacial advances during the LGM at sites across Patagonia that span a north-south transect of the Patagonian Ice Sheet may be related to a number of controlling factors, which operate at regional or hemispheric scales. The differences in the topography between the valleys have been suggested to control the style and timings of glacial advances (e.g. Glasser and Jansson, 2005). Overdeepening of the valleys east of the Patagonian Ice Sheet over time caused by the topographically-controlled, fast-flowing glaciers (e.g. Lago Buenos Aires) could potentially change the distribution of the ice volume so that the lateral extension of the glacial advance is reduced during larger but later glaciations (Kaplan et al., 2009). Evidence of glacial advances may also not be preserved in all the valleys, especially where

overridden by younger glacial advances (e.g. as suspected for MIS 4 glacial advances at Lago Buenos Aires). The glaciofluvial sediments in this study dated to 30.8 ± 5.7 ka (LBA12F4-2) and 34.0 ± 6.1 ka (sample LBA12RF1) provide a good example of these issues as similar aged deposits have rarely been reported from other sites in Patagonia, likely because of the lack of preservation and/or discovery.

For glacial advances at similar latitudes to have been synchronous across Patagonia but vary at different latitudes, large-scale shifts in climate may be controlling glaciation more than regional factors. Boex et al. (2013) have suggested that inconsistencies between glacial advances at different latitudes in Patagonia are related to the precipitation supply controlled by the migration of the Southern Westerlies during the LGM. During the LGM the Southern Westerlies expanded northwards and so the core is reported to have been located ~45–50 °S (Hulton et al., 1994; Denton et al., 1999). Positioning of the Southern Westerlies at latitudes ~45–50 °S would have increased the input of precipitation to the piedmont glacier at Lago Buenos Aires (~46 °S) and may have facilitated ice expansion at Lago Buenos Aires at this time but not in the rest of Patagonia. However, more evidence is required to substantiate this hypothesis.

8. Conclusions

Luminescence dating of proglacial samples from Lago Buenos Aires (~46 °S), east of the Northern Patagonian Icefield, provides rare evidence in Patagonia for glacial advance (s) during MIS 3 (~31–37 ka). Evidence of the oldest moraines preserved at Lago Buenos Aires from the LGM (MIS 2) is recorded from ~25 ka, in phase with LGM advances in the Strait of Magellan and Bahia Inútil, but out-of-phase with the LGM at Lago Pueyrrédon and the Chilean Lake District. Multiple fluctuations in glacial extent are then recorded at Lago Buenos Aires from ~17 to 23 ka by three advances, which are in phase with glacial advances that occurred at different latitudes across Patagonia (e.g. Lago Pueyrrédon, Strait of Magellan and Bahia Inútil). In contrast, the timing of the final glacial advance of the LGM preserved at Lago Buenos Aires (~15 ± 2 ka) was out-of-phase with the rest of Patagonia. The palaeoenvironmental records suggest that glacial conditions could have persisted in Patagonia up to ~15 ka and so the discrepancy in timings of glacial advances across Patagonia is either related to the lack of preservation of sediments at some sites, or regional discrepancies in climate during deglaciation.

Overall, luminescence dating using single grains of K-feldspar has excellent potential to contribute towards the ever increasing geochronological dataset constraining the timings of glacial advances in the Patagonian region. Improving and increasing these datasets will continue to advance our understanding of the synchronicity of glacial advances across Patagonia, and then begin to unravel the potential signature of past climatic changes on these dynamic systems.

Acknowledgements

Financial support for the work contributing towards this paper was provided by a NERC PhD studentship to RKS (NE/I1527845/1). We would like to thank N. Pearce for his assistance with the geochemical analyses, and S. Tooth and R. Robinson for their feedback on this research. The authors would like to acknowledge the assistance of M. Kaplan with re-calculating the cosmogenic isotope ages in this study and his comments on the manuscript. Guido Vittone is thanked for his assistance with fieldwork logistics in Argentina. Aberystwyth Luminescence Research Laboratory (ALRL) benefited from being part of the Climate Change Consortium for Wales (C3W). Stephan Harrison is thanked for his comments on this manuscript.

Appendix A. Supplementary data

Supplementary data related to this article can be found at http://dx.doi.org/10.1016/j.quascirev.2015.12.010.

References

Alexanderson, H., Murray, A.S., 2012. Luminescence signals from modern sediments in a glaciated bay, NW Svalbard. Quat. Geochronol. 10, 250–256.
Arnold, L.J., Roberts, R.G., 2009. Stochastic modelling of multi-grain equivalent dose (D_e) distributions: implications for OSL dating of sediment mixtures. Quat. Geochronol. 4, 204–230.
Auclair, M., Lamothe, M., Huot, S., 2003. Measurement of anomalous fading for feldspar IRSL using SAR. Radiat. Meas. 37, 487–492.
Balco, G., Stone, J.O., Lifton, N.A., Dunai, T.J., 2008. A complete and easily accessible means of calculating surface exposure ages or erosion rates from ^{10}Be and ^{26}Al measurements. Quat. Geochronol. 3, 174–195.
Balescu, S., Lamothe, M., 1993. Thermoluminescence dating of the Holsteinian marine formation of Herzeele, northern France. J. Quat. Sci. 8, 117–124.
Berger, G.W., Luternauer, J.J., 1987. Preliminary field work for thermoluminescence dating studies at the Fraser River delta, British Columbia. Geol. Surv. Can. Pap. 87 (IA), 901–904.
Berger, A., Loutre, M.F., 1991. Insolation values for the climate of the last 10000000 years. Quat. Sci. Rev. 10, 297–317.
Blombin, R., Murray, A., Thomsen, K.J., Buylaert, J.-P., Sobhati, R., Jansson, K.N., Alexanderson, H., 2012. Timing of the deglaciation in southern Patagonia: testing the applicability of K-feldspar IRSL. Quat. Geochronol. 10, 264–272.
Boex, J., Fogwill, C., Harrison, S., Glasser, N.F., Hein, A., Schnabel, C., Xu, S., 2013. Rapid thinning of the Late Pleistocene Patagonian ice sheet followed migration of the Southern Westerlies. Sci. Rep. 3, 1–6.
Bøtter-Jensen, L., Andersen, C.E., Duller, G.A.T., Murray, A.S., 2003. Developments in radiation, stimulation and observation facilities in luminescence measurements. Radiat. Meas. 37, 535–541.
Brook, E.J., White, J.W.C., Schilla, A.S.M., Bender, M.L., Barnett, B., Severinghaus, J.P., Taylor, K.C., Alley, R.B., Steig, E.J., 2005. Timing of millennial-scale climate change at Siple Dome, West Antarctica, during the last glacial period. Quat. Sci. Rev. 24, 1333–1343.
Buylaert, J.-P., Jain, M., Murray, A.S., Thomsen, K.J., Thiel, C., Sobhati, R., 2012. A robust feldspar luminescence dating method for Middle and Late Pleistocene sediments. Boreas 41, 435–451.
Caldenius, C.C., 1932. Las glaciaciones cuaternarios en la Patagonia y Tierra del Fuego. Geogr. Ann. 14, 1–164 (English summary, 144 – 157).
Chiverrell, R.C., Thrasher, I.M., Thomas, G.S.P., Lang, A., Scourse, J.D., van Landeghem, K.J.J., Mccarroll, D., Clark, C.D., Ó Cofaigh, C., Evans, D.J.A., Ballantyne, C.K., 2013. Bayesian modelling the retreat of the Irish Sea Ice Stream. J. Quat. Sci. 28, 200–209.
Darvill, C.M., Bentley, M.J., Stokes, C.R., Hein, A.S., Rodés, Á., 2015. Extensive MIS 3 glaciation in southernmost Patagonia revealed by cosmogenic nuclide dating of outwash sediments. Earth Planet. Sci. Lett. 429, 157–169.
Denton, G.H., Heusser, C.J., Lowell, T.V., Moreno, P.I., Andersen, B.G., Heusser, L.E., Schluchter, C., Marchant, D.R., 1999. Interhemispheric linkage of paleoclimate during the last glaciation. Geogr. Ann. 81A, 107–153.
Douglass, D.C., Singer, B.S., Kaplan, M.R., Mickleson, D.M., Caffee, M.W., 2006. Cosmogenic nuclide surface exposure dating of boulders on last-glacial and late-glacial moraines, Lago Buenos Aires, Argentina: interpretative strategies and paleoclimate implications. Quat. Geochronol. 1, 43–58.
Duller, G.A.T., 1992. Luminescence Chronology of Raised Marine Terraces Southwest North Island New Zealand. Unpublished PhD thesis. University of Wales, Aberystwyth.
Duller, G.A.T., 2000. Dose-distributions determined from measurements of single-grain quartz. In: Proceedings of International Symposium on Luminescence and its Applications, India (ISLA-2000), 1, pp. 78–85.
Duller, G.A.T., 2006. Single grain optical dating of glacigenic deposits. Quat. Geochronol. 1, 296–304.
Duller, G.A.T., 2008. Single-grain optical dating of quaternary sediments: why aliquot size matters in luminescence dating. Boreas 37, 589–612.
Duller, G.A.T., 2012. Improving the accuracy and precision of equivalent doses determined using the optically stimulated luminescence signal from single grains of quartz. Radiat. Meas. 47, 770–779.
Duller, G.A.T., Bøtter-Jensen, L., Murray, A.S., 2003. Combining infrared- and green-laser stimulation sources in single-grain luminescence measurements of feldspar and quartz. Radiat. Meas. 37, 543–550.
Espinoza, F., Morata, D., Polve, M., Lagabrielle, Y., Maury, R.C., de la Rupelle, A., Guivel, C., Cotten, J., Bellon, H., Suárez, M., 2010. Middle Miocene calc-alkaline volcanism in Central Patagonia (47 °S) petrogenesis and implications for slab dynamics. Andean Geol. 37, 300–328.
Fuchs, M., Owen, L.A., 2008. Luminescence dating of glacial and associated sediments: review, recommendations and future directions. Boreas 37, 636–659.
Gaar, D., Lowick, S.E., Preusser, F., 2014. Performance of different luminescence

approaches for the dating of known-age glaciofluvial deposits from northern Switzerland. Geochronometria 41, 65–80.
Galbraith, R.F., Roberts, R.G., 2012. Statistical aspects of equivalent dose and error calculation and display in OSL dating: an overview and some recommendations. Quat. Geochronol. 11, 1–27.
Glasser, N.F., Jansson, K.N., 2005. Fast-flowing outlet glaciers of the Last Glacial Maximum Patagonian Icefield. Quat. Res. 63, 206–211.
Glasser, N.F., Harrison, S., Jansson, K., Kleman, J., 2008. The glacial geomorphology and Pleistocene history of southern South America between 38°S and 56°S. Quat. Sci. Rev. 27, 365–390.
Glasser, N.F., Jansson, K.N., Goodfellow, B.W., de Angelis, H., Rodnight, H., Rood, D.H., 2011. Cosmogenic nuclide exposure ages for moraines in the Lago San Martin Valley, Argentina. Quat. Res. 75, 636–646.
Glasser, N.F., Harrison, S., Schnabel, C., Fabel, D., Jansson, K., 2012. Younger Dryas and early Holocene age glacier advances in Patagonia. Quat. Sci. Rev. 58, 7–17.
Godfrey-Smith, D.I., Huntley, D.J., Chen, W.-H., 1988. Optical dating studies of quartz and feldspar sediment extracts. Quat. Sci. Rev. 7, 373–380.
Guerin, G., Mercier, N., Adamiec, G., 2011. Dose-rate conversion factors: update. Anc. TL 29, 5–8.
Hein, A.S., Hulton, N.R.J., Dunai, T.J., Sugden, D.E., Kaplan, M.R., 2010. The chronology of the Last Glacial Maximum and deglacial events in central Argentine Patagonia. Quat. Sci. Rev. 29, 1212–1227.
Hulton, N.R.J., Sugden, D.E., Payne, A.J., Clapperton, C.M., 1994. Glacier modelling and the climate of Patagonia during the last glacial maximum. Quat. Res. 42, 1–19.
Huntley, D.J., Lamothe, M., 2001. Ubiquity of anomalous fading in K-feldspars and the measurement and correction for it in optical dating. Can. J. Earth Sci. 38, 1093–1106.
Imbrie, J., Hays, J.D., Martinson, D.G., Mcintyre, A., Mix, A.C., Morley, J.J., Paces, N.G., Prell, W.L., Shackleton, N.J., 1984. The orbital theory of Pleistocene climate: support from a revised chronology of the marine $\delta^{18}O$ record. In: Berger, A., et al. (Eds.), Milankovitch and Climate, Part. D. Reidel, Norwell, Mass, pp. 269–305.
Jain, M., Ankjærgaard, C., 2011. Towards a non-fading signal in feldspar: insight into charge transport and tunnelling from time-resolved optically stimulated luminescence. Radiat. Meas. 46, 292–309.
Jain, M., Murray, A.S., Bøtter-Jensen, L., 2004. Optically stimulated luminescence dating: how significant is incomplete light exposure in fluvial environments? Quaternaire 15, 143–157.
Kaiser, J., Lamy, F., Hebbeln, D., 2005. A 70-kyr sea surface temperature record off southern Chile (Ocean Drilling Program Site 1233). Palaeoceanography 20, PA4009.
Kaplan, M.R., Ackert, R.P., Singer, B.S., Douglass, D.C., Kurz, M.D., 2004. Cosmogenic nuclide chronology of millennial-scale glacial advances during O-isotope stage 2 in Patagonia. Geol. Soc. Am. Bull. 116, 308–321.
Kaplan, M.R., Douglass, D.C., Singer, B.S., Ackert, R.P., Caffee, M.W., 2005. Cosmogenic nuclide chronology of pre-last glaciation maximum moraines at Lago Buenos Aires, 46 °S, Argentina. Quat. Res. 63, 301–315.
Kaplan, M.R., Fogwill, C.J., Sugden, D.E., Hulton, N.R.J., Kubik, P.W., Freeman, S.P.H.T., 2008. Southern Patagonian glacial chronology for the Last Glacial period and implications for Southern Ocean climate. Quat. Sci. Rev. 27, 284–294.
Kaplan, M.R., Hein, A.S., Hubbard, A., Lax, S.M., 2009. Can glacial erosion limit the extent of glaciation? Geomorphology 108, 172–179.
Kaplan, M.R., Strelin, J.A., Schaefer, J.M., Denton, G.H., Finkel, R.C., Schwartz, R., Putnam, A.E., Vandergoes, M.J., Goehring, B.M., Travis, S.G., 2011. In-situ cosmogenic ^{10}Be production rate at Lago Argentino, Patagonia: implications for late-glacial climate chronology. Earth Planet. Sci. Lett. 309, 21–32.
Lambert, F., Delmonte, B., Petit, J.R., Bigler, M., Kaufmann, P.R., Hutterli, M.A., Stocker, T.F., Ruth, U., Steffensen, J.P., Maggi, V., 2008. Dust-climate couplings over the past 800,000 years from the EPICA Dome C ice core. Nature 452, 616–619.
Lamy, F., Kilian, R., Arz, H.W., Francois, J.-P., Kaiser, J., Prange, M., Steinke, T., 2010. Holocene changes in the position and intensity of the southern westerly wind belt. Nat. Geosci. 3, 695–699.
McCulloch, R.D., Bentley, M.J., Tipping, R.M., Clapperton, C.M., 2005. Evidence for Late-glacial ice dammed lakes in the central Strait of Magellan and Bahia Inutil, southernmost South America. Geogr. Ann. 87, 335–362.
Mercer, J.H., 1976. Glacial history of southernmost South America. Quat. Res. 6, 125–166.
Mercer, J.H., Sutter, J.F., 1982. Late Miocene-earliest pliocene glaciation in southern Argentina: implications for global ice sheet history. Paleogeogr. Paleoclimatol. Paleoecol. 38, 185–206.
Mix, A.C., Bard, E., Schneider, R., 2001. Environmental processes of the ice age: land, oceans, glaciers (EPILOG). Quat. Sci. Rev. 20, 627–657.
Murray, A.S., Thomsen, K.J., Masuda, N., Buylaert, J.P., Jain, M., 2012. Identifying well-bleached quartz using the different bleaching rates of quartz and feldspar luminescence signals. Radiat. Meas. 47, 688–695.
Prescott, J.R., Hutton, J.T., 1994. Cosmic ray and gamma ray dosimetry for TL and ESR. Nucl. Tracks Radiat. Meas. 14, 223–227.
Putnam, A.E., Schaefer, J.M., Barrell, D.J.A., Vandergoes, M., Denton, G.H., Kaplan, M.R., Finkel, R.C., Schwartz, R., Goehring, B.M., Kelley, S.E., 2010. In situ cosmogenic ^{10}Be production-rate calibration from the Southern Alps, New Zealand. Quat. Geochronol. 5, 392–409.
Putnam, A.E., Schaefer, J.M., Denton, G.H., Barrell, D.J.A., Birkel, S.D., Andersen, B.G., Kaplan, M.R., Finkel, R.C., Schwartz, R., Doughty, A.M., 2013. The last glacial maximum at 44°S documented by a ^{10}Be moraine chronology at Lake Ohau, Southern Alps of New Zealand. Quat. Sci. Rev. 62, 114–141.
Reimann, T., Thomsen, K.J., Jain, M., Murray, A.S., Frechen, M., 2012. Single-grain dating of young sediment using the pIRIR signal from feldspar. Quat. Geochronol. 11, 28–41.
Rhodes, E.J., 2011. Optically stimulated luminescence dating of sediments over the past 200,000 years. Annu. Rev. Earth Planet. Sci. 39, 461–488.
Roberts, H.M., 2012. Testing post-IR IRSL protocols for minimising fading in feldspars, using Alaskan loess with independent chronological control. Radiat. Meas. 47, 716–724.
Sagredo, E.A., Moreno, P.I., Villa-Martínez, R., Kaplan, M.R., Kubik, P.W., Stern, C.R., 2011. Fluctuations of the Última Esperanza ice lobe (52°S), Chilean Patagonia, during the last glacial maximum and termination 1. Geomorphology 125, 92–108.
Singer, B.S., Ackert, R.P., Guillou, H., 2004. $^{40}Ar/^{39}Ar$ and K–Ar chronology of Pleistocene glaciations in Patagonia. GSA Bull. 116, 434–450.
Smedley, R.K., 2014. Testing the Use of Single Grains of K-feldspar for Luminescence Dating of Proglacial Sediments in Patagonia (Ph.D. thesis). Aberystwyth University, U.K.
Smedley, R.K., Duller, G.A.T., 2013. Optimising the reproducibility of measurements of the post-IR IRSL signal from single-grains of feldspar for dating. Anc. TL 31, 49–58.
Smedley, R.K., Duller, G.A.T., Pearce, N.J.G., Roberts, H.M., 2012. Determining the K-content of single-grains of feldspar for luminescence dating. Radiat. Meas. 47, 790–796.
Smedley, R.K., Duller, G.A.T., Roberts, H.M., 2015. Assessing the bleaching potential of the post-IR IRSL signal for individual grains of K-feldspar: implications for single-grain dating. Radiat. Meas. 79, 33–42.
Thiel, C., Buylaert, J.-P., Murray, A., Terhorst, B., Hofer, I., Tsukamoto, S., Frechen, M., 2011. Luminescence dating of the stratzing loess profile (Austria) – testing the potential of an elevated post-IR IRSL protocol. Quat. Int. 234, 23–31.
Thomsen, K.J., Murray, A.S., Jain, M., Bøtter-Jensen, L., 2008. Laboratory fading rates of various luminescence signals from feldspar-rich sediment extracts. Radiat. Meas. 43, 1474–1486.
Thomsen, K.J., Murray, A.S., Jain, M., 2011. Stability of IRSL signals from sedimentary K-feldspar samples. Geochronometria 38, 1–13.
Thrasher, I.M., Mauz, B., Chiverrell, R.C., Lang, A., 2009a. Luminescence dating of glaciofluvial deposits: a review. Earth Sci. Rev. 97, 133–146.
Thrasher, I.M., Mauz, B., Chiverrell, R.C., Lang, A., Thomas, G.S.P., 2009b. Testing an approach to OSL dating of Late Devensian glaciofluvial sediments of the British Isles. J. Quat. Sci. 24, 785–801.
Trauerstein, M., Lowick, S.E., Preusser, F., Schlunegger, F., 2014. Small aliquot and single-grain IRSL and post-IR IRSL dating of fluvial and alluvial sediments from the Pativilca valley, Peru. Quat. Geochronol. 22, 163–174.
Turner, K.J., Fogwill, C.J., McCulloch, R.D., Sugden, D.E., 2005. Deglaciation of the eastern flank of the North Patagonian Icefield and associated continental-scale lake diversions. Geogr. Ann. 87A, 363–374.
Wallinga, J., Murray, A., Duller, G., 2000. Underestimation of equivalent dose in single-aliquot optical dating of feldspars caused by preheating. Radiat. Meas. 32, 691–695.
Wintle, A.G., 1973. Anomalous fading of thermoluminescence in mineral samples. Nature 245, 143–144.
Wintle, A.G., Murray, A.S., 2006. A review of quartz optically stimulated luminescence characteristics and their relevance in single-aliquot regeneration dating protocols. Radiat. Meas. 41, 369–391.